

Flow and Heat Transfer Characteristics in a Seven Tube-Bundle Wrapped with Helical Wires

T. Sreenivasulu*, BVSSS Prasad

Department of Mechanical Engineering, IIT Madras, Chennai-600036, India

E-mail addresses: chittoorreddy@gmail.com (Sreenivasulu), prasad@iitm.ac.in (Prasad)

Abstract

Local flow and heat transfer characteristics in a seven tube bundle helically wrapped with wires of circular cross section are obtained computationally and presented. Regions of sweeping and mixing flows and hot spots are identified from the local characteristics. Parametric investigations with varying outer diameter ratio ($D/d = 3.93, 4.24$ and 4.54), helical pitch ratio ($P/d = 9.09, 18.18$ and 30.30) and triangular pitch ratio ($P_t/d = 1.28, 1.32$ and 1.36) are presented for a Reynolds number range of 8,000 to 100,000. The average friction factors and Nusselt numbers show highest values for $D/d = 3.93$, $P/d = 9.09$ and $P_t/d = 1.36$. The variation of thermal hydraulic performance ratio against the mass flow rate provides an optimum geometry for the design of heat exchanger with seven tube bundle.

Key words: Flow and heat transfer, seven tube bundles, helically wrapped wire, augmentation, CFD.

Nomenclature

C1-C6	Corner Zones	
D	Outer diameter-----	m
D_ω	Cross diffusion term in turbulence	
d	Inner diameter-----	m
E	Energy-----	W
E1-E6	Edge Zones	
f	Friction factor	
G	Dimensionless generation term of turbulence	
I	Unit tensor	
I1-I6	Interior Zones	
k	Thermal conductivity-----	W/mK
Nu	Nusselt number	
P	Helical pitch length-----	m
p _o	Pressure -----	Pa
q	Heat flux-----	W/m ²
Re	Reynolds number	
S	Dimensionless source term in Turbulence	
T	Temperature-----	K
V	Velocity-----	m/sec
x	local axial distance-----	m

Y	Dimensionless dissipation term of turbulence
y^+	Viscous grid spacing
Greek Symbols	
Δ	Difference
κ	Turbulent kinetic energy ----- m^2/s^2
μ	Dynamic viscosity-----Pa-sec
Ω	Vorticity magnitude-----1/s
ω	Specific Dissipation rate-----1/s
ρ	Density----- kg/m^3
τ	Shear stress----- N/m^2
∇	Gradient operator

Subscripts

average	Average magnitude
axial	Magnitude of axial component
h	Hydraulic
in	Inlet
local	Local magnitude
max	Maximum
rad	Magnitude of radial component
tan	Magnitude of tangential component
w	Wrap-wire
κ	Turbulent kinetic energy
ω	Specific dissipation rate

Abbreviations

SDR	Specific dissipation rate
TKE	Turbulent Kinetic energy
THPR	Thermal hydraulic performance ratio

1. Introduction

Design of most shell and tube heat exchangers is primarily governed by shell side pressure drop and heat transfer rates. In general, any method to augment heat transfer entails increase in pressure drop as well. An improved understanding of the flow and heat transfer behavior in the core region of heat exchangers for different geometric parameters may therefore lead to optimum designs with improved thermal-hydraulic performance.

In a recent article Sreenivasulu and Prasad [1] suggested that the external surface of the heat exchanger tubes might be wrapped with helical wires for better thermal hydraulic performance. They demonstrated the advantage by estimating a parameter called Thermal Hydraulic Performance Ratio (THPR) for an annulus that may simulate a parallel pipe heat exchanger. An optimum parametric combination could be chosen for a given cylindrical annulus wrapped with helical wire.

The present paper envisages the use of tubes wound helically on their external surface for heat exchanger applications. The wire wrapped geometries were earlier experimentally studied in the context of nuclear thermal hydraulics. For instance, Bishop and Todreas [2]

presented the velocity distributions and a model to calculate friction factors. Chun and Seo [3] and Bubelis and Schikorr [4] compiled correlations for friction factor in helically wrapped wire rod bundles. By comparing the available correlations with the experimental data, Chun and Seo concluded that among several available correlations, the one suggested by Cheng and Todreas [5] is the best, whereas Bubelis and Schikorr [4] concluded that Rehme [9] correlation is the best one. Table 1 shows the correlations for friction factors for wire wrapped bundle. The exhaustive literature on friction factors notwithstanding, very little information is available on heat transfer in the wire-wrapped bundle in the open literature. Fenech and co-workers [11, 18] presented a comprehensive experimental study and recommended the following correlations for Nusselt number based on their experimental study.

$$\text{Nu} = 0.0136 (\text{Re})^{0.75} (\text{Pr})^{1.08} \quad \text{for Re} < 1100$$

$$\text{Nu} = 0.0248 (\text{Re})^{0.79} (\text{Pr})^{0.43} \quad \text{for } 1100 < \text{Re} < 10^4$$

The computational works based on multi-dimensional modeling for the estimation of friction factors and heat transfer coefficients in the wire wrapped geometries are recent and very limited [19, 20]. These methods are essentially developed for the rod-bundles in reactor assemblies. The work reported by Gajapathy *et al.* [19] is perhaps the first to report the multidimensional modeling. They used commercial CFD for wire-wrapped seven-rod bundle geometry and applied k- ϵ turbulence model. More recently Raza and Kim [20] compared three cross sectional shapes of the wire, *viz.*, the circular, hexagonal and rhombus and concluded that the last geometry gives the highest overall pressure drop as well as heat transfer rates.

The scope of each of the earlier computational investigations was limited to any one geometric configuration and hence is not adequate for an understanding of the parametric effects such as diameter ratios, helical pitch ratios and triangular pitch ratios, on the behavior of friction factor and Nusselt numbers. The current paper aims at presenting the (i) computational fluid dynamic methodology and results of the local flow and temperature patterns, friction factors and Nusselt numbers for different geometric variations of a wire-wrapped seven-tube core of a shell and tube type heat exchanger and (ii) evaluating shell-side thermal hydraulic performance ratio for the geometry.

2. Physical Model and Meshing

The physical configuration and computational domain in Fig. 1 is a helically wire wrapped core of a seven-tube heat transfer bundle. The same dimensions of the inner tube and wire-wrap, as used in wire-wrapped annuli [1], are adopted in generating the solid model for the wire-wrapped seven-tube bundle. The cusp approximation used in the wire-wrapped annuli is extended for the bundle. However the same cooper algorithm used in [1] cannot be implemented as the outer shell is chosen to be of hexagon shape. Therefore, tetrahedral mesh is first generated for the wire-wrapped bundles up to one sixth of the pitch length, corresponding to the 60 degree rotation of the wrap-wire refer Fig.2. This mesh is rotated and repeated six times by making use of the hexagonal rotational symmetry to obtain finer mesh. A non-conformal method is used to connect these six domains. The mesh size for the wire-

wrapped tube bundle is chosen around 3 million after the grid independence study with mesh size varying from 0.3 to 4 million cells. In these domains, fine clustered mesh near the walls is generated and care is taken such that the value of wall y^+ does not exceed five; refer to the inset of Fig.2. Table.2 gives the details of different configurations, their mesh size and the maximum wall y^+ , these mesh sizes are chosen after a proper grid independence study and an extra care has been taken on mesh quality of all the simulation files. All the simulations are carried out using commercial code Fluent (version 6.3).

3. Methodology

The differential equations governing the flow, turbulence and heat transfer under the assumptions of steady, incompressible flow are given as follows:

Conservation of mass:

$$(\nabla \cdot (\rho \vec{v})) = 0 \quad (1)$$

Conservation of momentum:

$$\nabla \cdot (\rho \vec{v} \vec{v}) = -\nabla p + \nabla \cdot (\overline{\tau}) + \rho \vec{g} \quad (2)$$

The stress tensor $\overline{\tau}$ is given by

$$\overline{\tau} = \mu \left[(\nabla \vec{v} + \nabla \vec{v}^T) - \frac{2}{3} \nabla \cdot \vec{v} I \right] \quad (3)$$

where the second term on the right hand side is the effect of volume dilation. For incompressible flow, $[\nabla \cdot \vec{v} I]$ becomes zero.

Conservation of Energy:

$$\nabla \cdot (\vec{v} (\rho E + p)) = \nabla \cdot \left(k_{eff} \nabla T - \sum_j h_j \vec{J}_j + (\overline{\tau}_{eff} \cdot \vec{v}) \right) \quad (4)$$

Where k_{eff} the effective conductivity = $k + k_t$, where k_t is the turbulent thermal conductivity, defined according to the turbulence model being used. The first three terms on the right-hand side of Equation (4) represent energy transfer due to conduction, species diffusion, and viscous dissipation respectively.

TKE equation:

$$\frac{\partial}{\partial t} (\rho \kappa) + \frac{\partial}{\partial x_i} (\rho \kappa u_i) = \frac{\partial}{\partial x_j} \left(\Gamma_\kappa \frac{\partial \kappa}{\partial x_j} \right) + G_\kappa - Y_\kappa + S_\kappa \quad (5)$$

SDR equation:

$$\frac{\partial}{\partial t}(\rho\omega) + \frac{\partial}{\partial x_i}(\rho\omega u_i) = \frac{\partial}{\partial x_j} \left(\Gamma_\omega \frac{\partial \omega}{\partial x_j} \right) + G_\omega - Y_\omega + D_\omega + S_\omega \quad (6)$$

Where the $\Gamma_\kappa = \mu + \frac{\mu_t}{\sigma_\kappa}$, $\Gamma_\omega = \mu + \frac{\mu_t}{\sigma_\omega}$ where

$$\sigma_{\kappa,1} = 1.176, \sigma_{\omega,1} = 2.0, \sigma_{\kappa,2} = 1.0, \sigma_{\omega,2} = 1.168 .$$

All these equations are solved using Fluent (Version 6.3) [21] finite volume commercial code. Implicit second order upwind scheme is used for solving the above equations. The convergence criterion is fixed such that the residual values are lower than 10^{-6} . The pressure correction approach using the SIMPLE algorithm is used. Mass flow rate is specified at the inlet whereas static pressure is given at the outlet. Static temperature of the fluid (ambient value) is specified at the inlet. Water is used as fluid in the present analysis. These input conditions are estimated indirectly from the chosen Reynolds number value. The same input conditions are given as initial conditions for the present numerical computations. An adiabatic and no slip wall boundary are assumed for the outer wall of the annulus. Uniform heat flux condition is applied for the outer wall of the inner cylinder. The temperature difference between surfaces of helical wire and the inner cylinder are assumed to be negligible. This means that a conjugate analysis due to presence of conduction across the surfaces is not necessitated. Thus the same heat flux values imposed on inner cylinder are applicable for the helical wrap-wire surface as well. The turbulence model is chosen after applying various two-equation turbulence models available in the software. Whilst all the turbulence models have yielded same results for bare annuli, the turbulence model has significant influence on the results of wire-wrapped annuli. It has been found by experimenting with different turbulence models, that the best model for is k- ω SST as it has predicted the flow in the wake of the cylinder very well. It is also evident from the literature [22] that k- ω SST is perhaps the best among the RANS models when flow field contains swirling motion. In keeping with the above, the k- ω SST model is chosen for prediction of the turbulent flow hydrodynamics and transport rate in helically wire-wrapped bundle.

4. Results and Discussion

4.1 Validation:

The numerical results of the seven-tube wire-wrapped bundle are validated in two ways. First, the overall friction factors are compared with the experimental correlations of Cheng and Todreas [5] and Rehme [9], as shown in Fig.3. Second, the cross flow function defined as $(V_{\tan} / V \tan\theta)$ is estimated and compared with the experimental data of the same quantity measured using LDA by Basehore and George [23](data is taken for a corner zone from Roidt *et al.* [24]) Both these agree within 10%, refer to Fig. 4. The friction factor computed from the present computations agree within +15% of Rehme [9] and -10% with Cheng and Todreas [5], by considering the ambiguity of available literature, in correlations, it is considered that present simulation is validated.

4.2 Flow pattern

The path line patterns are shown in Figs.5 and 6 for the bare tube-bundle and for the wire-wrapped tube bundles respectively. The corner zones C1 to C6, Edge zones E1 to E6 and Interior zones I1 to I6 are shown marked by dotted line boundaries in these Figures. By comparing the path line pattern in different zones, the symmetric and cyclic nature of the flow is evident in the bare tube bundle. In other words, the pattern is similar in similar zones. The flow mixing and thermal characteristics are therefore expected to be similar zones of the bare bundle. However, it is obvious from Fig. 6 that this cyclic and symmetric nature is completely disturbed by the wire wraps. The asymmetric flow pattern is obvious even among the zones of similar type. Considering the differences in the flow pattern formed for different zones around the central tube, the mean flow in this core region is found to mix well around the central tube. In contrast, the flow in the outer region (near the hexagonal wall) is predominantly 'sweeping' in the upper zones: E1, E2, C1 and C2. On the other hand, it is predominantly 'mixing' in the lower zones E4, C4, E3 and C3. These differences are due to changing positions of the wrapped wires in the different zones. The continued change in the direction of wire wrap is responsible also for inducing large cross flow mixing, a contribution from the radial and tangential components of velocity. This will be discussed further in a later section.

Figures 7 and 8 present the local velocities in the tube bundles, normalized with the bundle average velocity. The bundle average velocity (V_{avg}) is lower for the bare bundle and is higher for the wire wrapped bundle due to the blockage created by the wire wraps. The local velocity in the bare bundle is predominantly axial. The magnitude of velocity is almost uniform except very close to the walls of the tubes. In other words strong velocity gradients are confined only close to the tube surfaces in bare bundle. Referring to Fig.8 and comparing it with Fig.6 asymmetric and highly skewed velocity pattern is noticed due to helical wire wrap. The sweeping flow region generally offers lower resistance to flow than the mixing flow region. Therefore the velocity values are relatively higher in the sweeping regime. On the other hand, more uniform velocity values occur in the mixing regime. The magnitude of velocity variations at a distance " r_{mid} " around each tube are plotted in Fig.9. The positions of helical wires wrapped around the tubes (corresponding to this result) are shown in the insert of the same figure. The magnitudes of velocity for wire-wrapped bundle are in general larger. However, the velocity of V_{local}/V_{avg} is not much different from the bare-bundle, except close to the wire. These velocity ratio variations change from one axial position to the other, depending on the wire location, and are somewhat similar to the ones explained for the wire-wrapped annulus in ref [19].

The contours of the axial velocity of bare and wire-wrapped bundle normalized with the respective average velocity values are shown in Figs.10 and.11 respectively. The axial velocity is larger in the edge zone, when compared to the corner and interior zone for both wrapped wire and bare bundle. The velocity in the interior zone is less compared to other zones due to higher resistance offered to the flow by the tubes. The magnitude of velocity is more in the front side of the wire compared to the aft side. The velocity values in the corner and the edge zone are almost the same.

The changes in the velocity vector pattern and in the normalized tangential velocity contours are depicted in Figs. 12 and 13. As the tangential velocity gradients are considered primarily

responsible for the increased wall friction and heat transfer, the obvious changes in the magnitudes of tangential velocity contours at respective locations are noteworthy. The changes in the velocity, close to the wire, are significant due to the cross flow and the wake created by the wire. The tangential velocity is also larger in the front side of the wire compared to its aft side of the wire. It is evident from Figs.12 and 13 that the maximum tangential velocity is around $\pm 15\%$ of the average velocity whereas it will be about $\pm 10\%$ in bare bundle. Further the regions of maximum tangential velocity are more wide-spread in the wire wrapped bundle.

Figures 14 and 15 present the local pressure variations in the tube bundle at $x/p=0.5$, normalized with the bundle average pressure. The bundle average pressure (P_{avg}) is lower and more uniform for the bare bundle and compared to that in the wire wrapped bundle due to the blockages created by the wire wraps. The pressure in the wire wrapped bundle is completely non-uniform in nature. The changes are clearly evident even in the same type of sub-zones viz. E1 to E6 or C1 to C6. Variations of these pressures in the same plane indicate that the mixing will be higher in the wrapped bundle.

Figure 16 shows the polar plots of pressure profiles normalized with average pressure around all seven tubes with and without wrapped wires. In the bare bundle the polar plot is a circle around each tube; signifying that the pressure variations for the bare bundle are too small; the ratio of maximum to minimum pressure is almost unity. It is clearly seen that the pressure profile around each tube is not only non-circular but is completely different among the seven tubes in the wrapped tube bundle. The distortion in the profile is more predominant in outer tubes compared to the center tube. In other words the distortion in the edge and corner sub-zones is more dominant compared to the interior zones. This can be explained from the path lines shown in Fig. 6; where it is shown that the 'sweeping flow' is more dominant in mixing the fluid and hence creating significant variations in pressure. It is also observed that the distortion in the pressure profile of the outer tubes (R2 to R7) is larger in the direction of rotation of wire. In the wire-wrapped bundle the pressure variation around each tube is also considerable, the maximum to minimum variations for tubes R1 to R7 are given by 1.28, 1.36, 1.37, 1.35, 1.32, 1.30, and 1.36 respectively. The pressure is higher on the front side of the wire compared to its aft side. This difference is again attributable to the differences in the flow patterns observed in Fig.6.

4.3 Temperature Distribution

The non-dimensional temperature ($\theta^* = (T - T_{in})X(\bar{q}''L/K)$) (where the heat flux parameter, $\bar{q}''L/k=2383.33 \text{ k}^{-1}$) contours of bare and wrapped wire tube bundles at a plane $x/p=1.0$ are shown in Figs.17 and 18. Typically this value of heat flux parameter translates to a rate of specific enthalpy rise at about 500 watts per meter length. The changes in the flow pattern also reflect the changes in the temperature distribution in the bundles. The loss of symmetry in the temperature contours and the differences of temperature within different-zones are some of the features noted akin to velocity patterns. Close to the tube, the tendency to develop hot spots is observed because the temperature in the front side of the wire is much larger compared to the back side of the wire, as shown in the inset of Fig.18. It is clearly seen from the figure that the temperature values are higher in the interior zones compared to edge

and corner zones. This difference can be attributed to two reasons: firstly, there is significant difference in mixing and sweeping flow patterns; secondly, all surrounding tubes contribute to the rise of temperature in the interior zone, whereas the walls do not contribute to rise in temperature for the edge/corner zones.

The heat flux parameter is chosen such that fluid does not 'boil' close to the cusp region. With this input rate, much closer to the wall, near to the cusp region, significant temperature variations up to 21% occurs. The cusp regions with high temperature gradients are important because phase change (if any) will be initiated here converting them to become critical hot spot zones. The maximum temperature value and the extent of hot spot zone increase with increase in input heat flux and decrease in mass flow rate. Figure 19 shows the polar plots of temperature profiles normalized with temperature around all seven tubes with and without wrapped wires. It is evident from the figure due to insertion of wire the uniformity or circularity in the temperature profile last and also this variation is not same for all the tubes as mentioned in previous sections.

4.4 Friction factor

Figure 20 shows the typical behavior of pressure drop at different mass flow rates for the bare and wire-wrapped bundles. For the same geometry, the dimensionless pressure drop (friction factor) is plotted against Reynolds number in Fig.21. It is evident that the friction factor of wire-wrapped bundle is large by about 17.40% compared to the bare bundle at a Reynolds number 8000. The same behavior is observed by Bubelis and Schikorr [4] as they compared various correlations for wrapped and bare bundles correlation. However, an apparently opposite trend is observed by Gajapathy et.al [19]. This qualitative difference is only due to different in the definitions of friction factor and the Reynolds number .

The curves shown in Figs. 22 to 24 depict the behavior of friction factor with Reynolds number for variations of (a) Diameter ratio (b) Pitch ratio (c) Triangular pitch ratio. It is obvious from these figures that D/d has slightly increasing influence on friction factor of wire wrapped bundle. As D/d increases, the flow area in the corner and edge zone increase, thereby increasing the flow rate and wall friction. In the present D/d range of 3.93 to 4.54, the friction factor exhibited an increase of 14.25% at Reynolds number of 10^6 .

As the helical pitch is reduced, the helical angle increases and consequently, the swirl component of velocity increase. This in turn increases the friction factor (Fig 23), The reduction in pitch ratio also leads to increase in mixing.

It is observed that among all the parameters the triangular pitch ratio (Fig.24) is most sensitive parameter which affects the friction factor. The increase in the triangular pitch results in the increase of the size of interior zone and hence reduces the size of edge and corner zones. These two parameters will have opposing effects on pressure drop. In the edge and corner zones pressure drop will be reduced mildly, whereas in interior zones it increases substantially. As a result, the overall pressure drop and friction factor values increase with increase in the triangular pitch ratio. The maximum deviation in friction factor among all triangular pitches is observed at low Reynolds numbers which is around 133%.

4.5 Nusselt Number

Figure 25 shows the comparison of Nusselt number between the bare bundle and wire wrapped bundle for a typical configuration. As expected the introduction of wire into the bare bundle results in increase in heat transfer as the wire acts as a turbulence promoter and a swirl generator. The swirl and turbulence generation leads to good mixing which results in increase in heat transfer. The Nusselt number values of the wrapped bundle are larger by about 61% at a Reynolds number of 10^6 when compared with bare bundle.

The curves shown in Figs 26 to 28 reveal the behavior of Nusselt number with Reynolds number for (a) diameter ratio (b) pitch ratio (c) triangular pitch ratio. There are several parameters simultaneously affecting the heat transfer in the wrapped wire tube bundles *viz.* tubes spacing, inter-zone cross flow, wire wrap effect so the behavior of the tube bundle. The increase in outer diameter (diameter of the circle inscribing the hexagonal sheath) resulted in an decrease in Nusselt number. Typically the maximum value of Nusselt number at $D/d=3.93$ is about 52% higher compared to the value at $D/d=4.52$. The decrease in pitch diameter ratio causes an increase in the swirl, turbulence and mixing. This results in increase of heat transfer. The increase in the helical angle also causes an increase in the boundary layer unsteadiness which in turn contributes to increase in heat transfer. The value of maximum Nusselt number at $p/d=9.09$ is about 60% higher compared to $p/d=30.30$ at a Reynolds number 30,000. The variation of Nusselt number with respect to triangular pitch is depicted in Fig. 28. The decrease in triangular pitch ratio shows the decrease in Nusselt number. The triangular pitch $Pt/d=1.36$ shows a maximum of 38.36 % compared to $Pt/d=1.28$.

4.6 Performance

The ratio of heat transfer rate between enhanced and reference surfaces $((Nu_w/Nu) / (f_w/f))$ under identical flow rate are used as the performance parameter for quantifying the augmentation. This parameter is named as thermal hydraulic performance ratio, THPR. The derivation of the above THPR is given by Fan *et.al* [25]. The values of THPR for different configurations used in the present analysis are shown in Fig. 29. All the configurations of wrapped wire tube bundle yield better performance compared to the bare tube bundle at all Reynolds numbers. It is clear from the figure that each design has its own best mass flow rate. Using the above map one can decide what type of design can be used corresponding to a chosen mass flow rate. For example, at a mass flow rate of 3 kg/sec $P/d=30.30$, $D/d=4.54$, $Pt/d=1.28$ is the best choice; but it is not so at a mass flow rate of 5kg/sec.

5. Conclusions

1. The computational methodology with $k-\omega$ SST model is established by comparing the results with the available literature values ([5], [9] and [22]).
2. The flow in the edge and corner zones (E1, E2, C1 and C2) are identified is region of mixing flow. The flow in the edge and corner zones (E4, C4, E3 and C3) zones are identified is region of sweeping flow. A likely hot spot zone is identified close to the cusp contact between the tube and the wire.
3. As compared to the bare bundle the tangential velocity (swirl), turbulence, pressure drop and Nusselt numbers are larger for the wire wrapped bundle. Typically, at Reynolds number of 10^6 , Nusselt number of wire wrapped bundle larger by about 61%.
4. The decrease in outer diameter ratio and pitch ratio and increase in triangular pitch ratio results in increase in friction factors and Nusselt numbers. The average friction factors and Nusselt numbers show highest values for $D/d=3.93$, $P/d=9.09$ and $Pt/d=1.36$.

5. The variation of thermal hydraulic performance ratio against the mass flow rate provides an optimum geometry for the design of heat exchanger with seven tube bundle.

Acknowledgement

One of the author (TS) gratefully acknowledges the financial assistance received from the Indira Gandhi Center for Atomic Research, Govt. of India – IIT Madras cell while undertaking the work.

References

- [1] Sreenivasulu T., Prasad B.V.S.S.S. Flow and heat transfer characteristics in an annulus wrapped with a helical wire, *International Journal of Thermal Sciences*, 48, (2009) 1377-1391.
- [2] Bishop A. A., Todreas N. Hydraulic characteristics of wire-wrapped rod bundles, *Nuclear Engineering and Design*, 62 (1980) 271-293.
- [3] Chun M.H., Seo K.W. An Experimental study and assessment of existing friction factor correlations for wire wrapped fuel assemblies, *Annals of Nuclear Energy*, 28 (2001) 1683-1695.
- [4] Bubelis E., Schikorr M. Review and proposal for best fit of wire-wrapped fuel bundle friction factor and pressure drop predictions using various existing correlations, *Nuclear Engineering and Design*, 238 (2008) 3299-3320.
- [5] Cheng S.K., Todreas N. Hydrodynamic models and correlations for bare and wire wrapped hexagonal rod bundle friction factors and mixing parameters, *Nuclear Engineering Design*, 92 (1986) 227-251.
- [6] Eifler W., Nijssing R. Experimental investigation of velocity distribution and flow resistance in a triangular array of parallel rods, *Nuclear Engineering and Design*, 5 (1967) 22-42.
- [7] Grillo P., Marinelli V. Single and two-phase pressure drop on a 16-rod bundle, *Nuclear Applications & Technology*, 9 (1970) 682-693.
- [8] Novendstern E.H. Turbulent flow pressure drop model for fuel rod assemblies utilizing a helical wire-wrap spacer system, *Nuclear Engineering and Design*, 22 (1972) 19–27.
- [9] Rehme K. Pressure drop correlations for fuel element spacers, *Nuclear Technology*, 17 (1972) 15-23.
- [10] Engel F. C. Markley R. A., Bishop A. A. Laminar, transition and turbulent parallel flow pressure drop across wire-wrap-spaced rod bundles, *Nuclear Science and Engineering*, 69 (1979) 290–296.
- [11] Arwlkar K., Fenech H. Heat Transfer, Momentum Losses and Flow Mixing In a 61-Tube Bundle with Wire-Wrap, *Nuclear Engineering and Design*, 55 (1979), 403-417
- [12] Carajilescov P., Elói Fernandez F.Y. Model for sub channel friction factors and flow redistribution in wire-wrapped rod bundles, *Journal of the Brazilian Society of Mechanical Sciences*, 21 (1999).
- [13] Vijayan P.K., Pilkhwal D.S., Saha D., Venkat Raj V. Experimental studies on the pressure drop across the various components of a PHWR fuel channel, *Experimental Thermal and Fluid Science*, 20 (2004) 34-44.
- [14] Choi S. K., Choi K., Nam H. Y., Choi J. H., Choi H. K. Measurement of pressure drop in a full-scale fuel assembly of a liquid metal reactor, *Journal Pressure Vessel Technology*, 125 (2003) 233–238.
- [15] Holloway M.V., McClusky L.H., Beasley D.E., Conner M.E. The effect of support grid Features on local, single-phase heat transfer measurements in rod bundles, *ASME Journal of heat transfer*, 126 (2004) 43-53.
- [16] Sobolev V. Fuel rod and assembly proposal for XT-ADS pre-design, In: Coordination meeting of WP1&WP2 of DM1 IP EUROTRANS, Bologna, February, 8–9, 2006.
- [17] Vijayan P.K., Pilkhwal D.S., Saha D., Venkat Raj V. Experimental investigation of pressure phase friction factor for bare bundle was compared with drop across various Components of AHWR, ISHMT, Guwahati. (2006)
- [18] Fenech H. Local Heat Transfer and Hot-Spot Factors In Wire-Wrap Tube Bundle, *Nuclear Engineering and Design*, 88 (1985), 357-365.
- [19] Gajapathy R., Velusamy K., P. Selvaraj, Chellapandi P., Chetal S.C. CFD investigation of helical wire-wrapped 7-pin fuel bundle and the challenges in modeling full scale 217 pin bundle, *Nuclear Engineering and Design*, 237 (2007) 2332-2342.
- [20] Raza W., Kim K.Y. Comparative analysis of flow and convective heat transfer between 7-pin and 19-pin wire-wrapped fuel assemblies, *Journal of Nuclear Science and Technology*, 45 (2008) 653-661.

- [21] Fluent (version 6.3) user manual
- [22] F.R. Menter, Two-equation eddy-viscosity turbulence models for engineering applications, *AIAA Journal*, 32 (1994) 269–289.
- [23] Basehore K.L., T.L. George, T.L. Transactions American Nuclear Society, 3 (1979) 826-827.
- [24] Rioldt R.M., Carelli M.D., Markley R.A. Experimental investigations of the hydraulic field in wire-wrapped LMFBR core assemblies, *Nuclear Engineering and Design*, 62 (1980) 295-321.
- [25] Fan J.F., Ding W.K., Zhang J.F., He Y.L., Tao W.Q. A performance evaluation plot of enhanced heat transfer techniques, *International Journal of Heat and Mass Transfer*, 52 (2008), 33-44

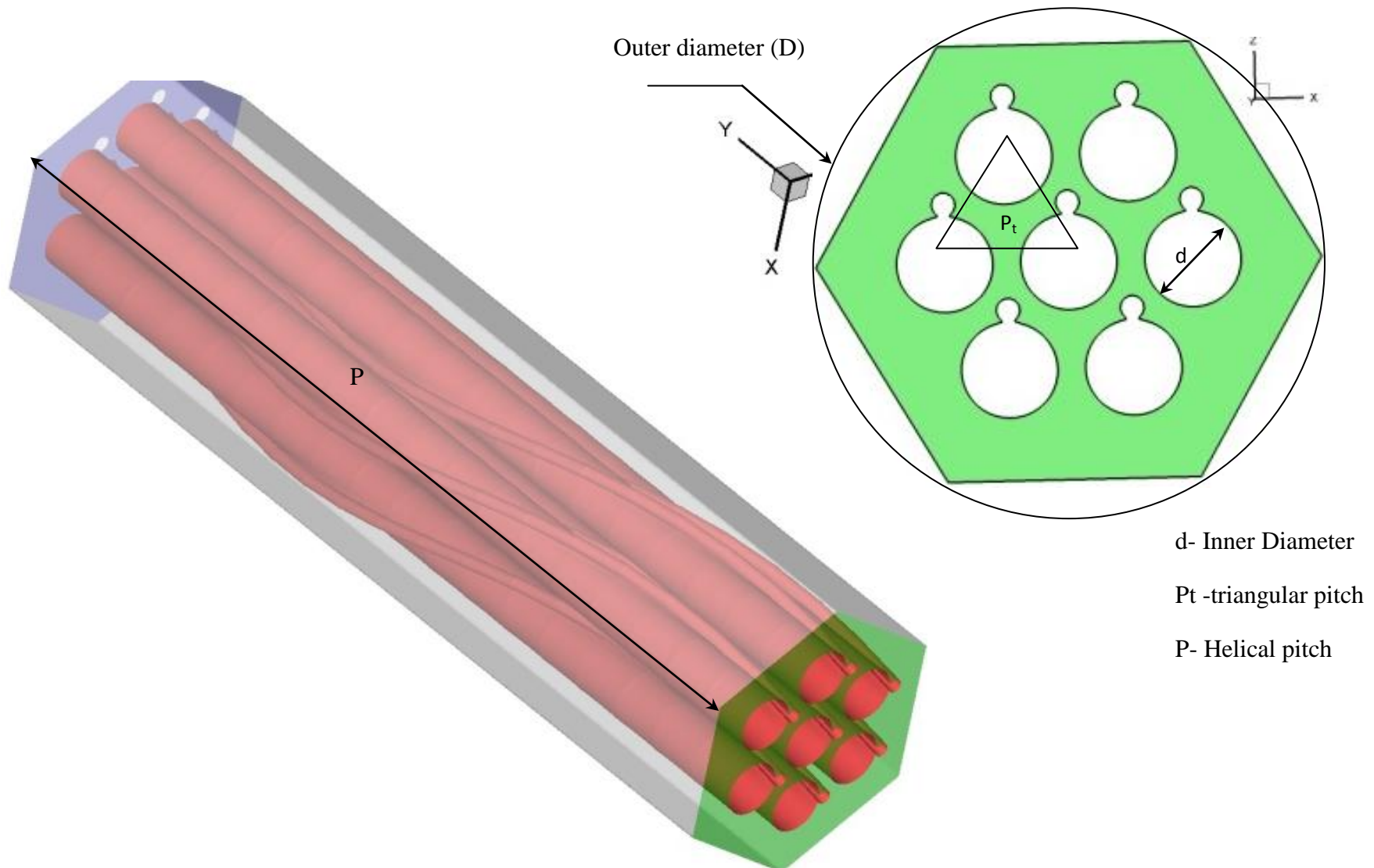


Fig.1 Computational domain of helically wire wrapped core of a seven-tube bundle

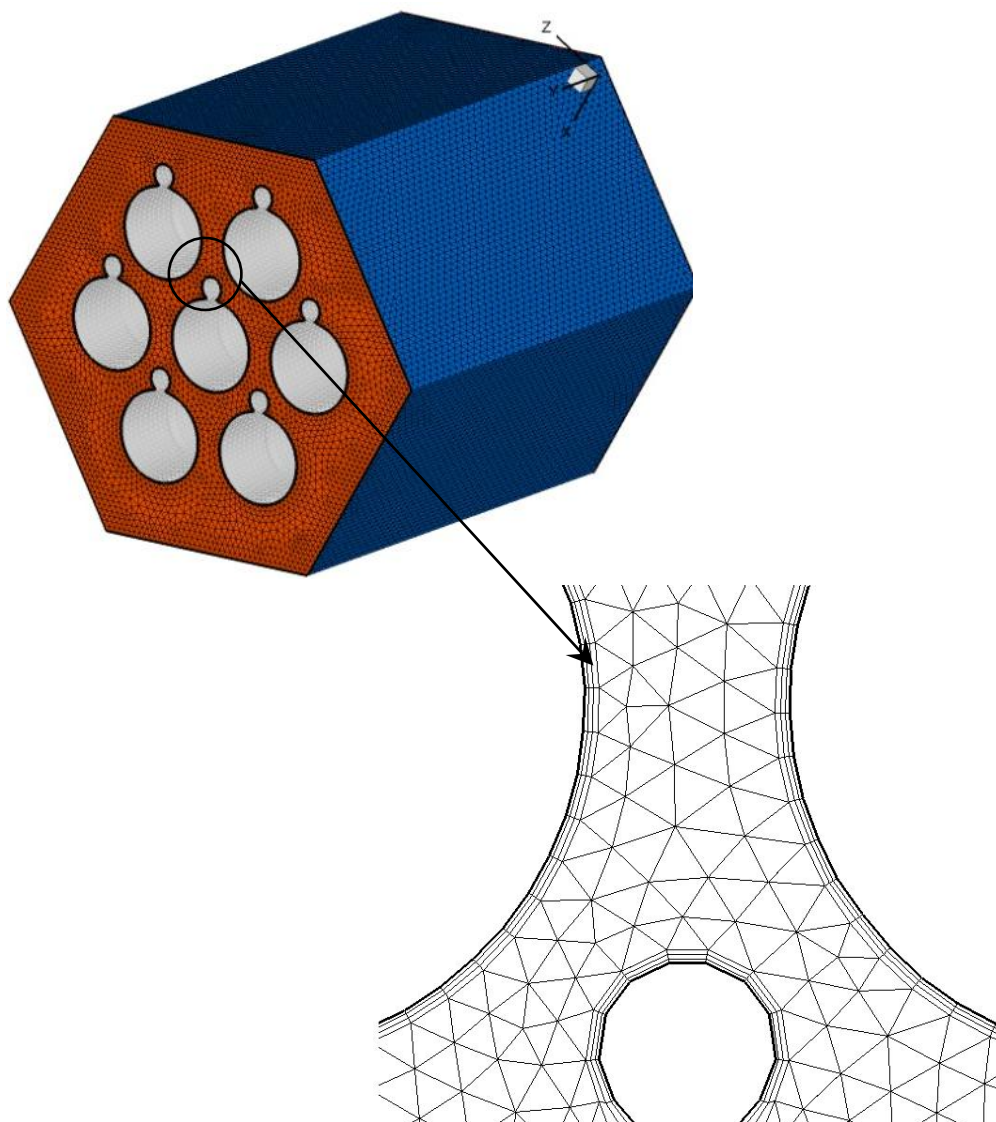


Fig.2 Tetrahedral mesh with clustering of grid near walls for wrapped wire seven tube bundle

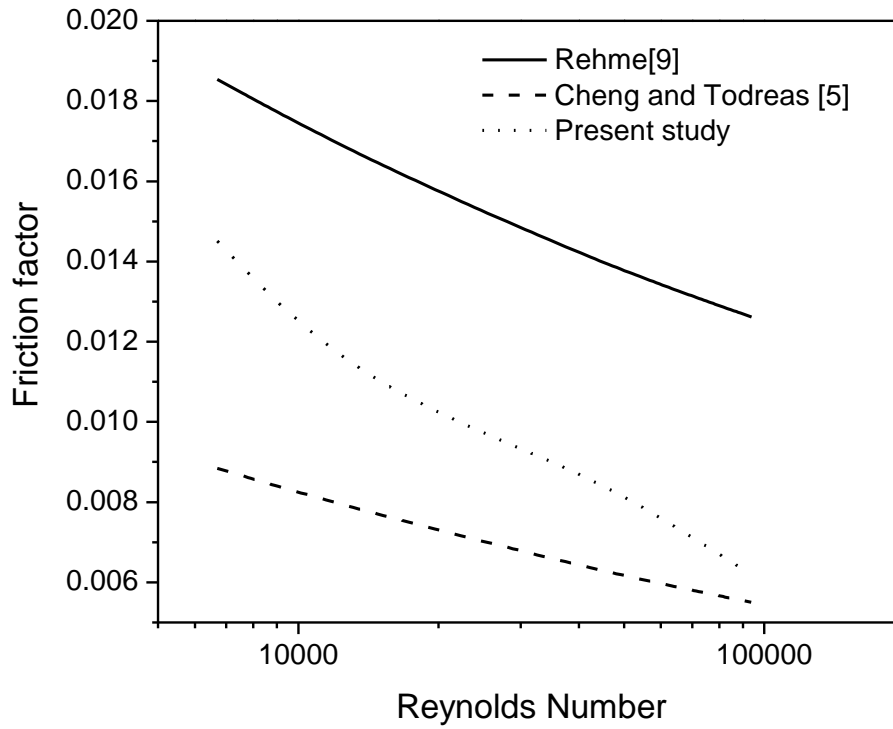


Fig.3 Comparison of present study friction factor with correlations available in literature

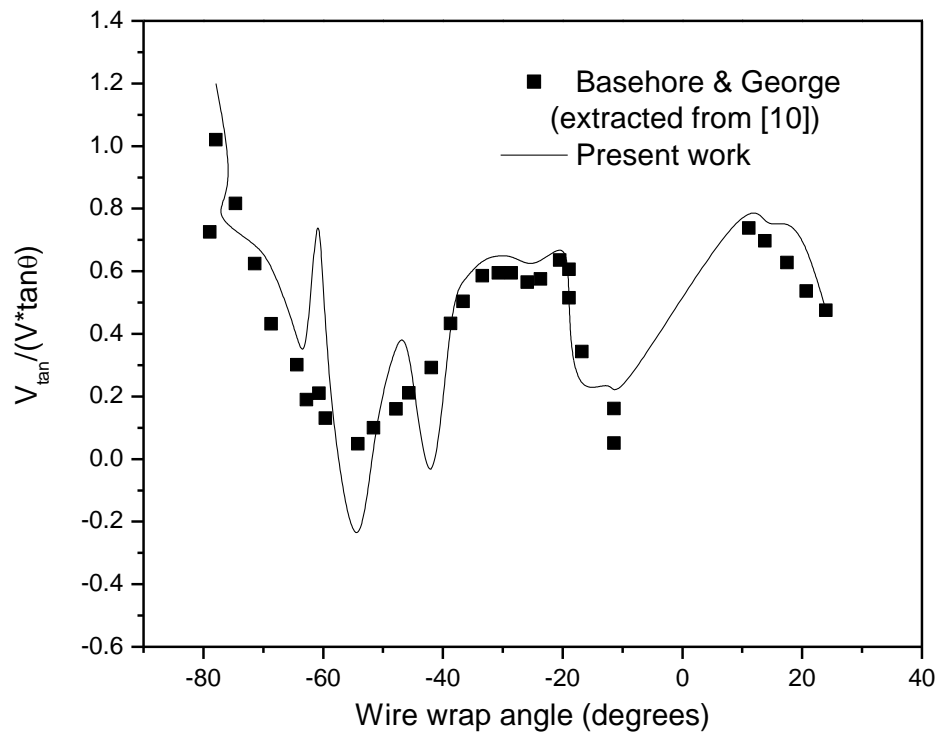


Fig.4 Comparison of present study cross flow function for corner zone from available literature

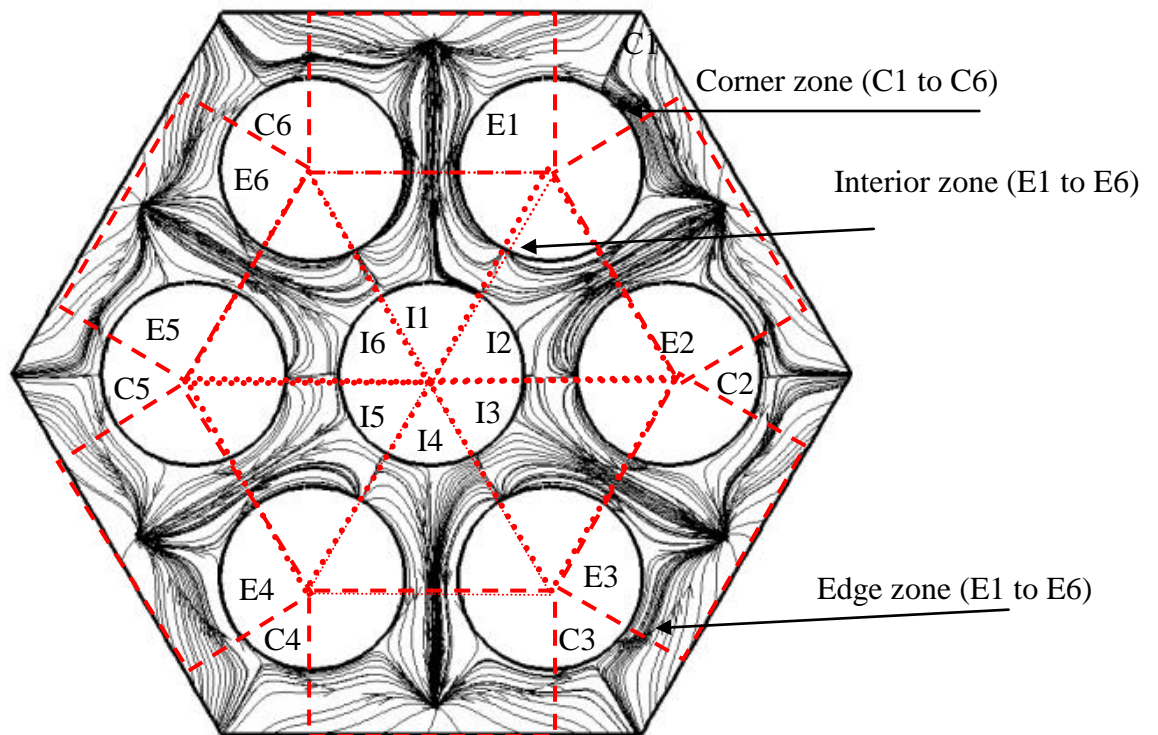


Fig.5 Path line pattern for bare tube bundle at an axial location of $x/p=0.5$ for the configuration of $P/d=30.30$, $P_p/d=1.34$ and $D/d=4.5$

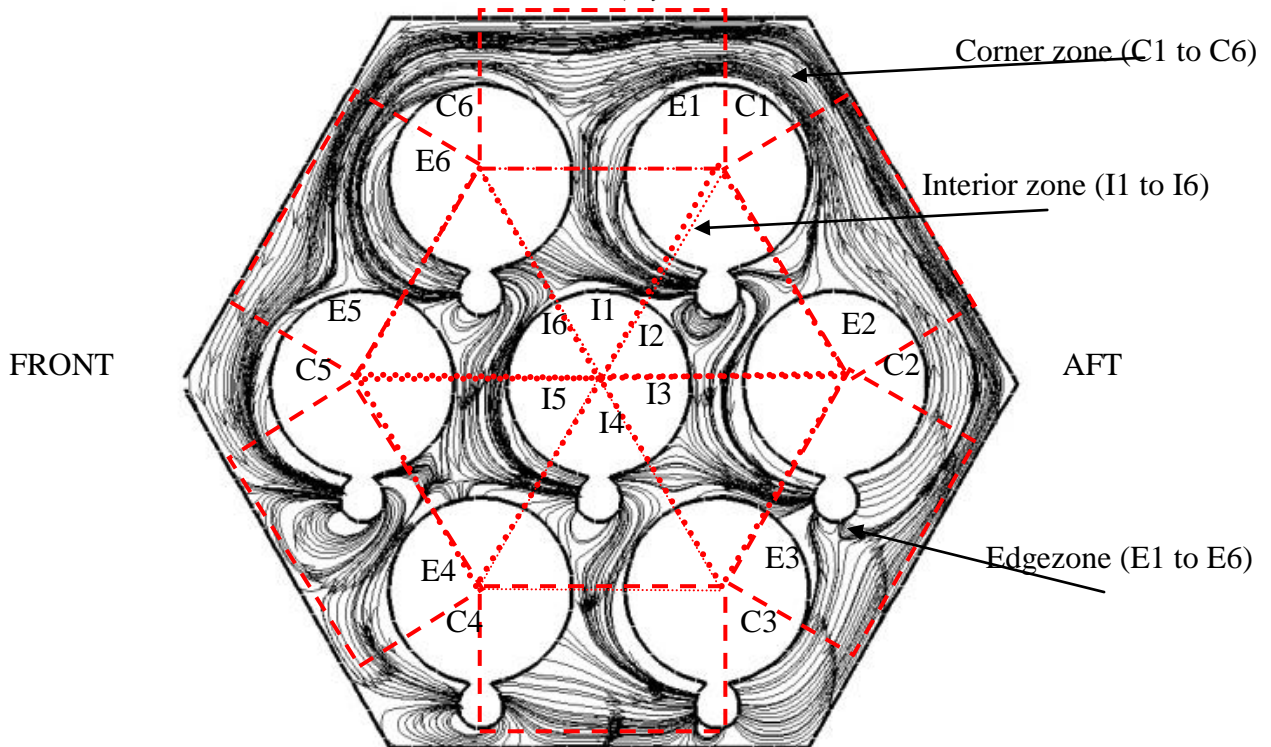


Fig.6 Path line pattern for wire-wrapped tube bundle at an axial location of $x/p=0.5$ for the configuration of $P/d=30.30$, $P_p/d=1.34$ and $D/d=4.5$

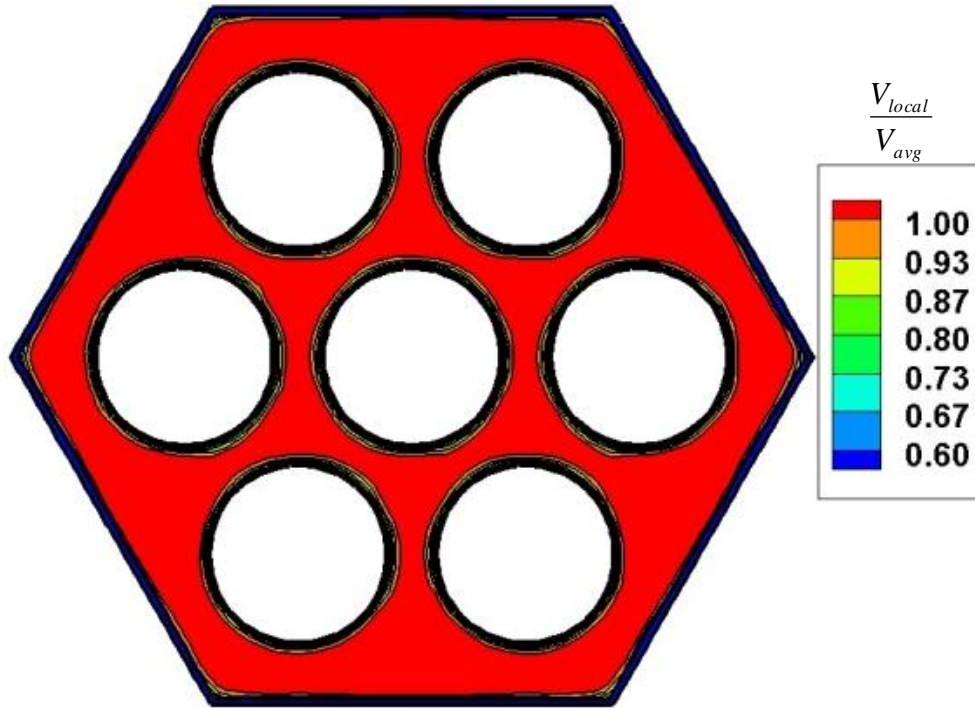


Fig.7 V_{local}/V_{avg} Contour for bare-wrapped tube bundle at an axial location of $x/p=0.5$ for the configuration of $P/d=30.30$, $P_v/d=1.34$, $D/d=4.5$

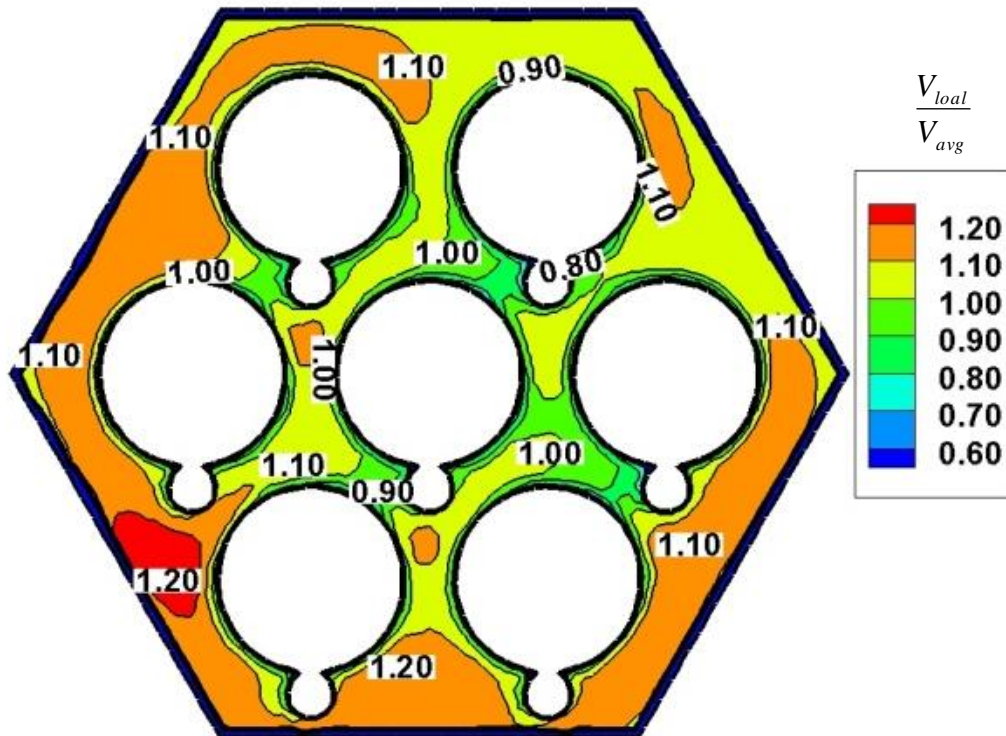


Fig.8 V_{local}/V_{avg} Contour for wire-wrapped tube bundle at an axial location of $x/p=0.5$ for the configuration of $P/d=30.30$, $P_v/d=1.34$, $D/d=4.5$

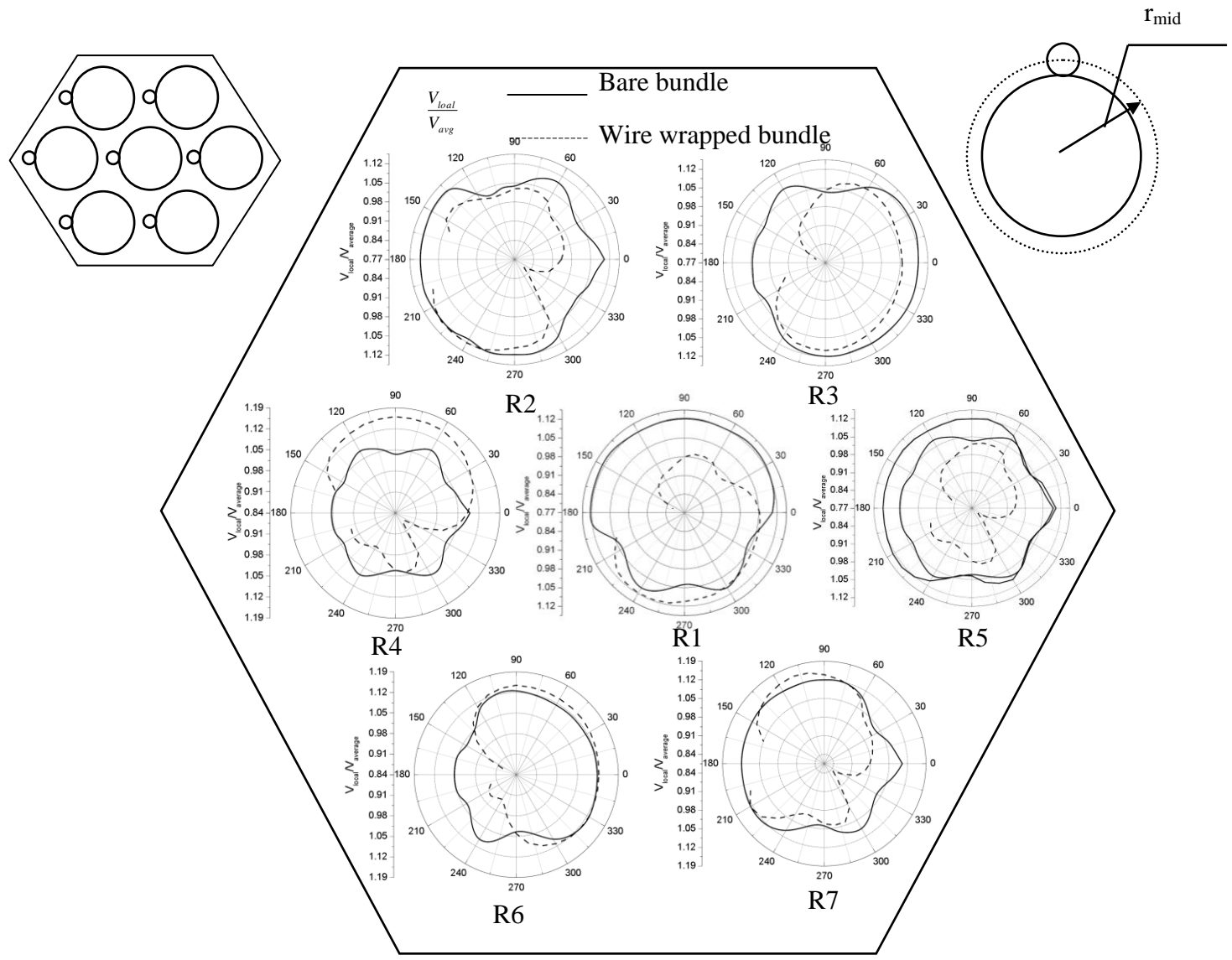


Fig.9 Comparison of V_{local}/V_{avg} distributions for wire-wrapped and bare tube bundle at axial location of $x/p=0.5$ and radial location of r_{mid} for the configuration of $P/d=30.30$, $P_t/d=1.34$, $D/d=4.5$

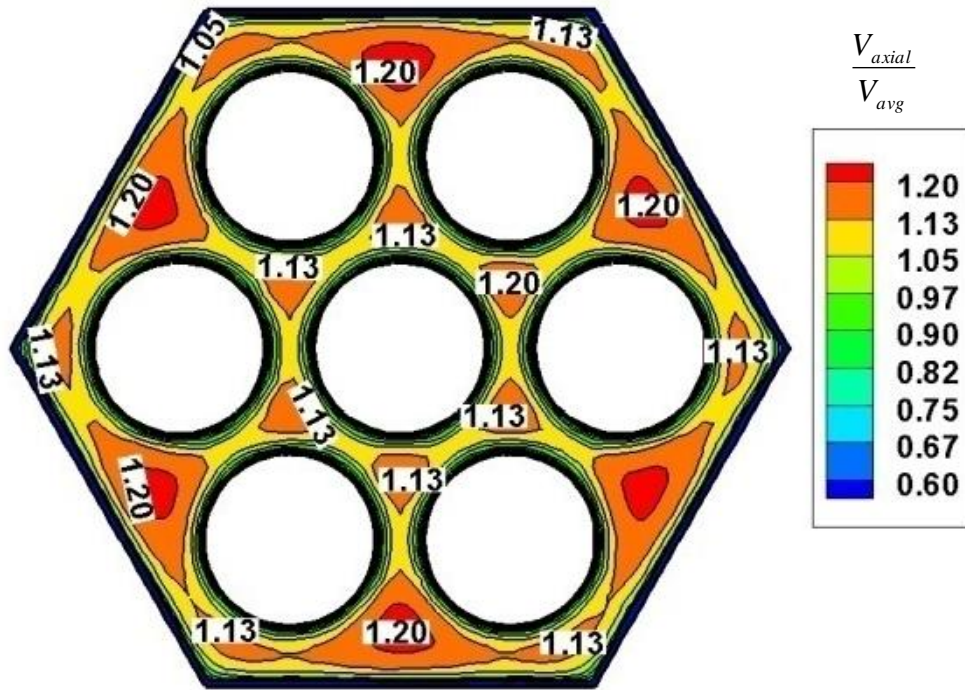


Fig.10 Contours of axial velocity component for bare tube bundle at axial location of $x/p=0.5$ for the configuration of $P/d=30.30$, $P_i/d=1.34$, $D/d=4.5$

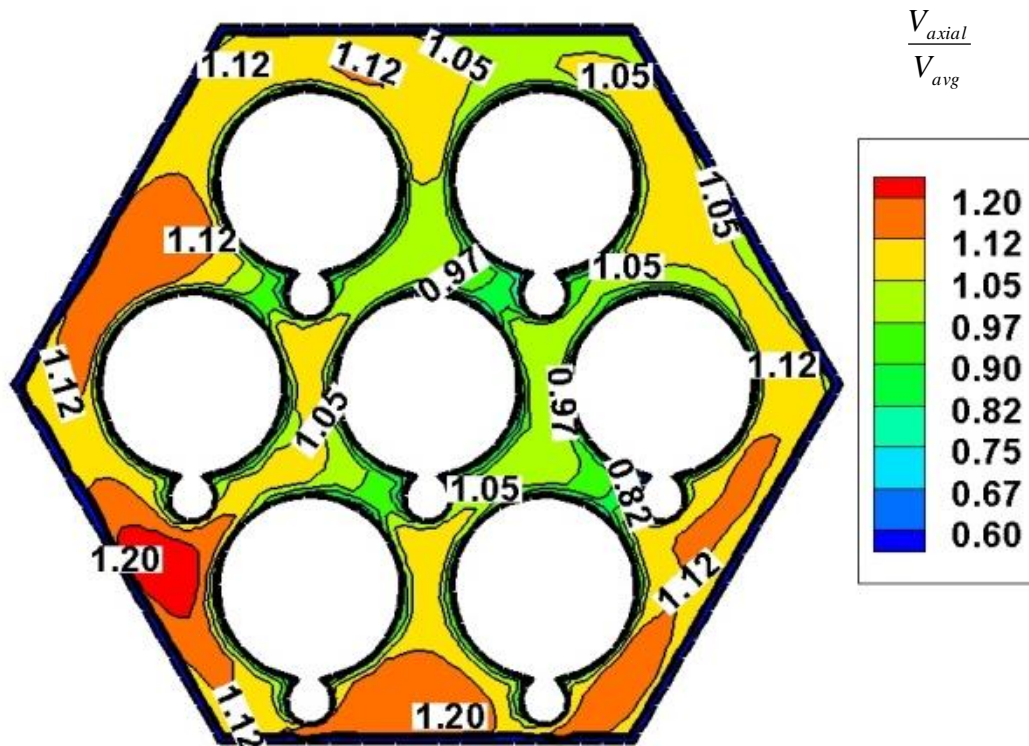


Fig.11 V_{axial}/\bar{V} contour for wire-wrapped tube bundle at axial location of $x/p=0.5$ for the configuration of $P/d=30.30$, $P_i/d=1.34$, $D/d=4.5$

$$\frac{V_{tan}}{V_{avg}}$$

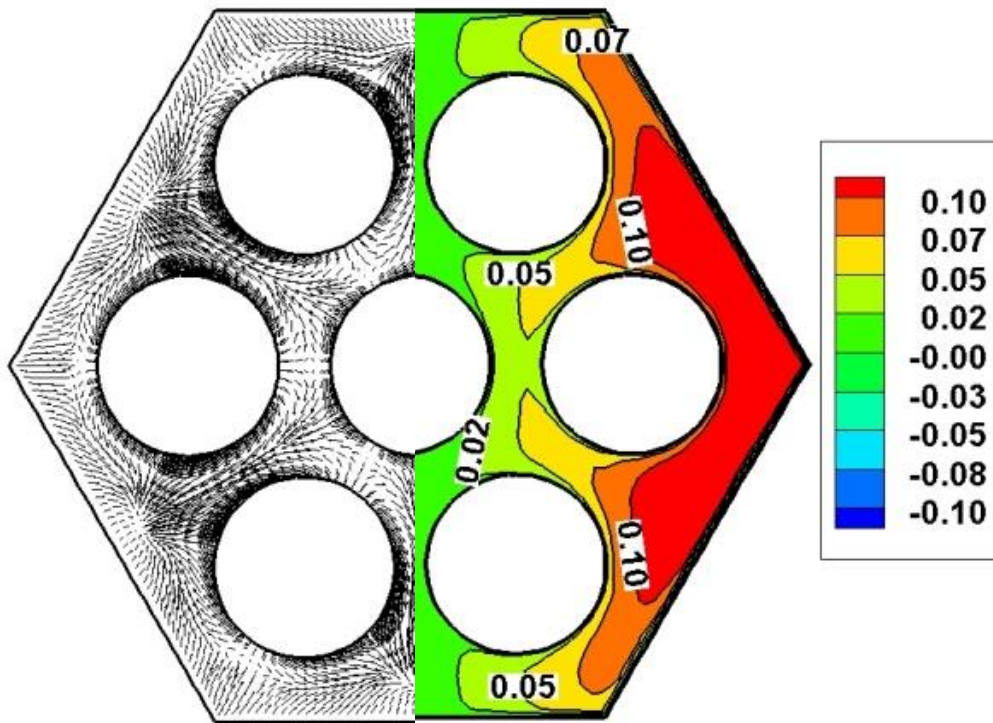


Fig.12 V_{tan}/\bar{V} contour and Velocity vector for bare tube bundle at axial location of $x/p=0.5$ for the configuration of $P/d=30.30$, $P_r/d=1.34$, $D/d=4.5$

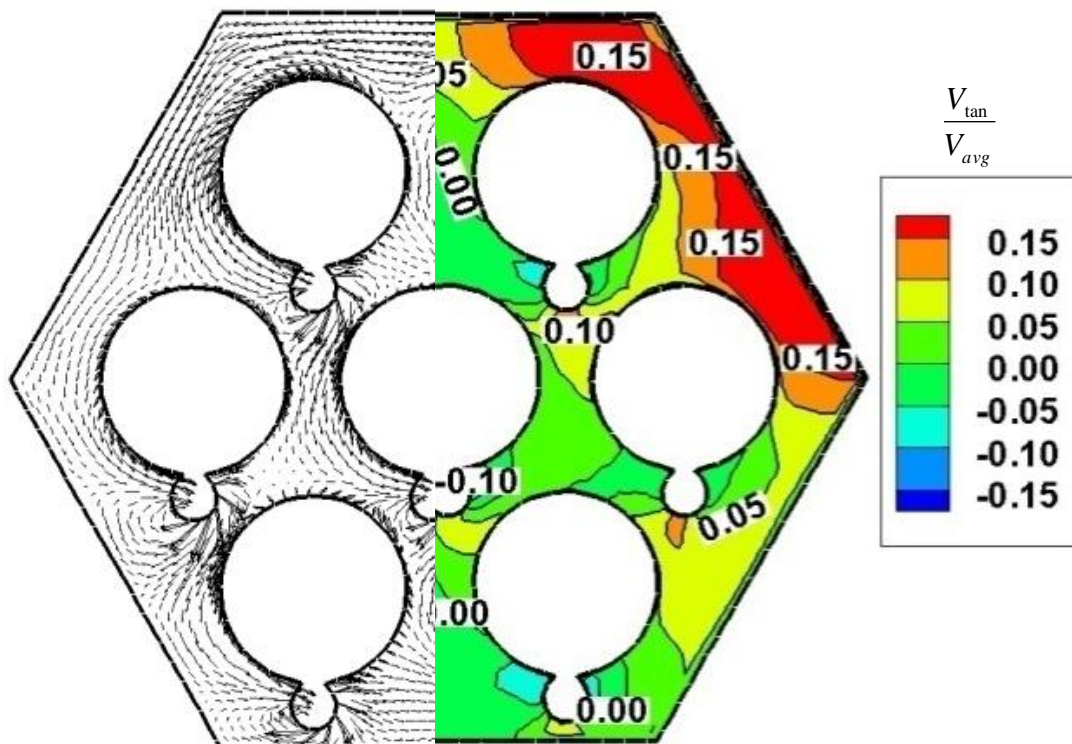


Fig.13 V_{tan}/\bar{V} contour and Velocity vector for wire-wrapped tube bundle at axial location of $x/p=0.5$ for the configuration of $P/d=30.30$, $P_r/d=1.34$, $D/d=4.5$

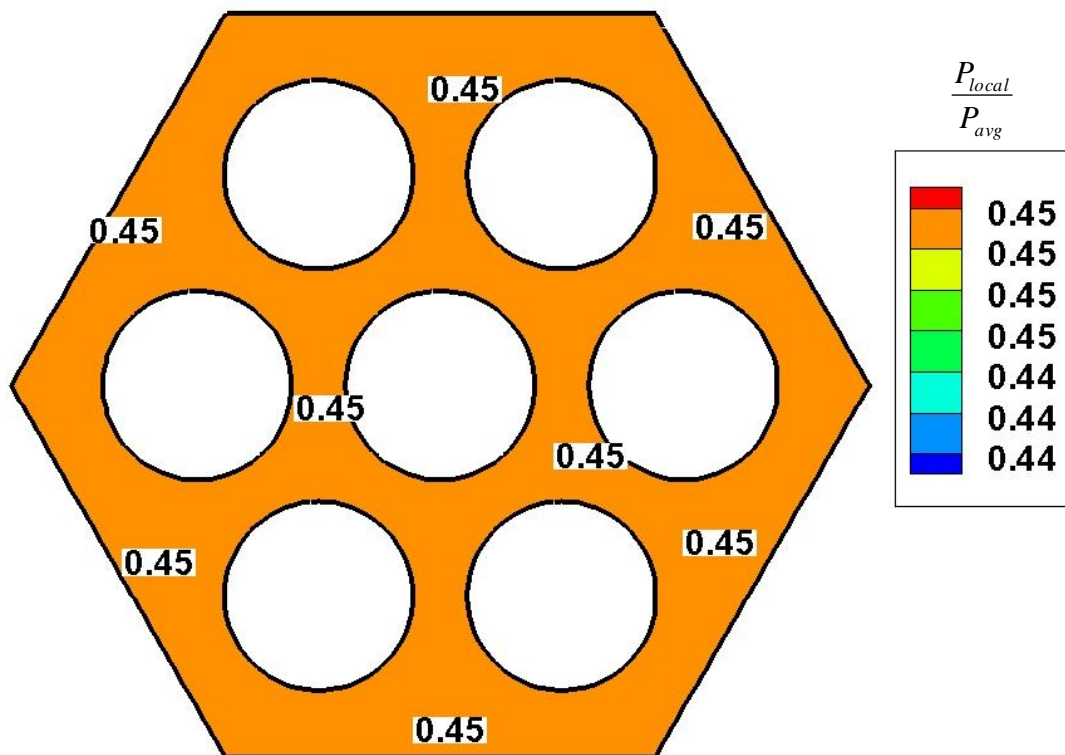


Fig.14 P_{local}/\bar{P} contour for wire-wrapped tube bundle at axial location of $x/p=0.5$ for the configuration of $P/d=30.30, P_i/d=1.34, D/d=4.5$

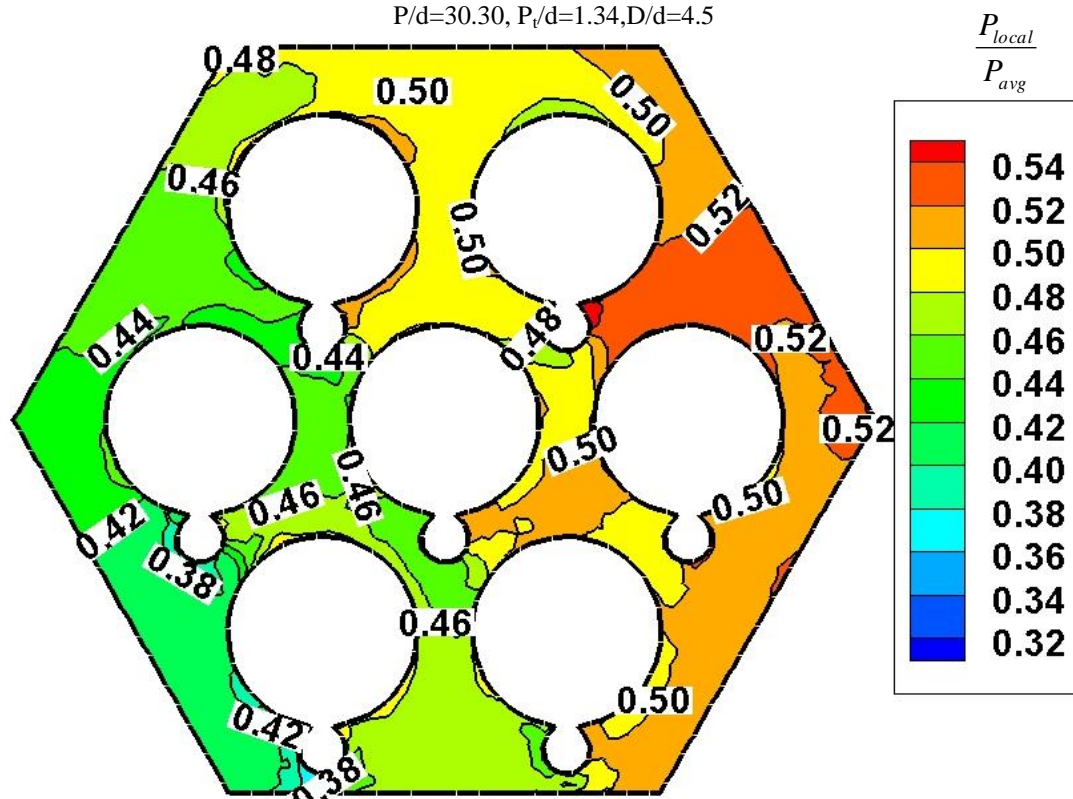


Fig.15 P_{local}/\bar{P} contour for wire-wrapped tube bundle at axial location of $x/p=0.5$ for the configuration of $P/d=30.30, P_i/d=1.34, D/d=4.5$

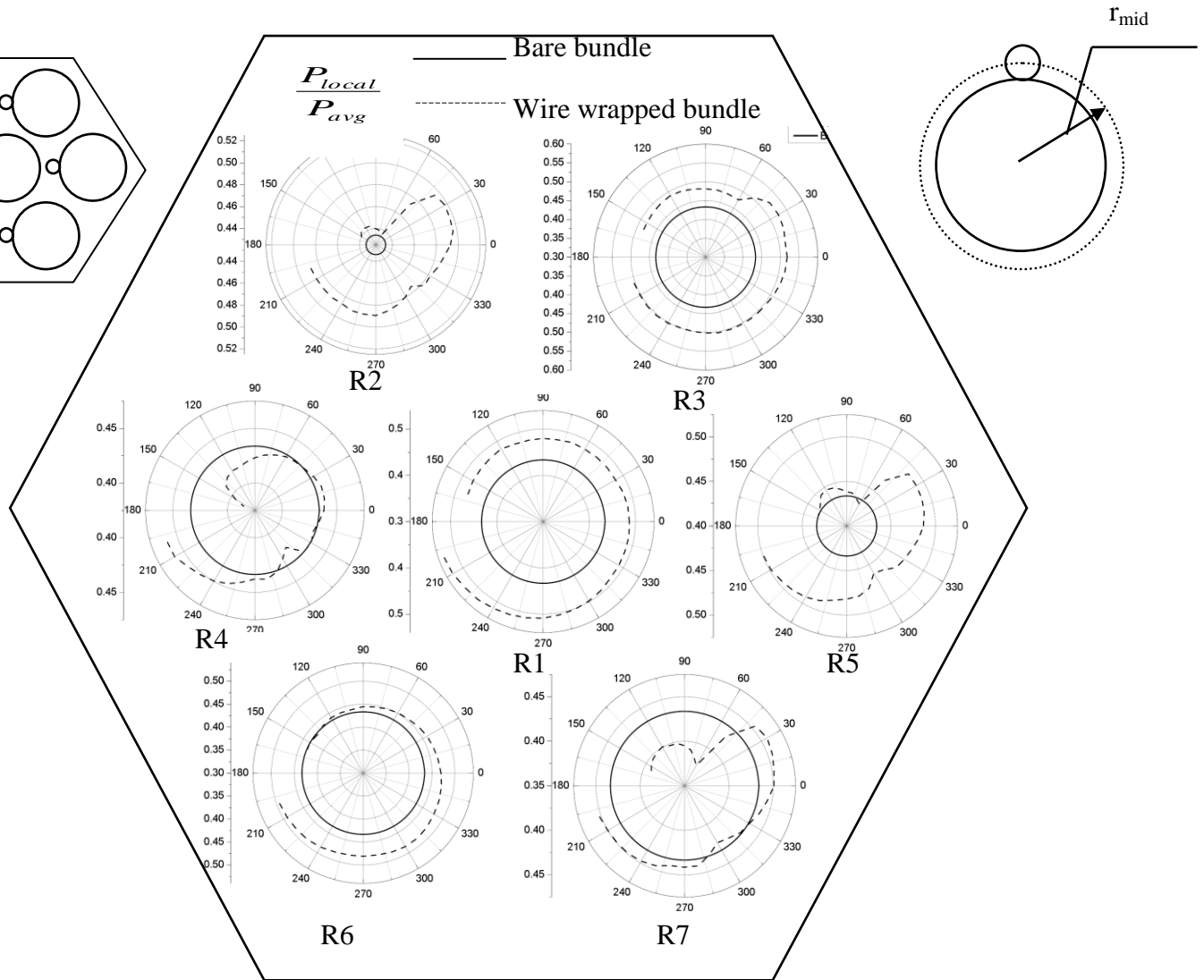


Fig.16 Comparison of P_{local}/P_{avg} distributions for wire-wrapped & bare tube bundle at axial location of $x/p=0.5$ and radial location of mid of the helically wrapped wire diameter for the configuration of $P/d=30.30$, $P_t/d=1.34$, $D/d=4.5$

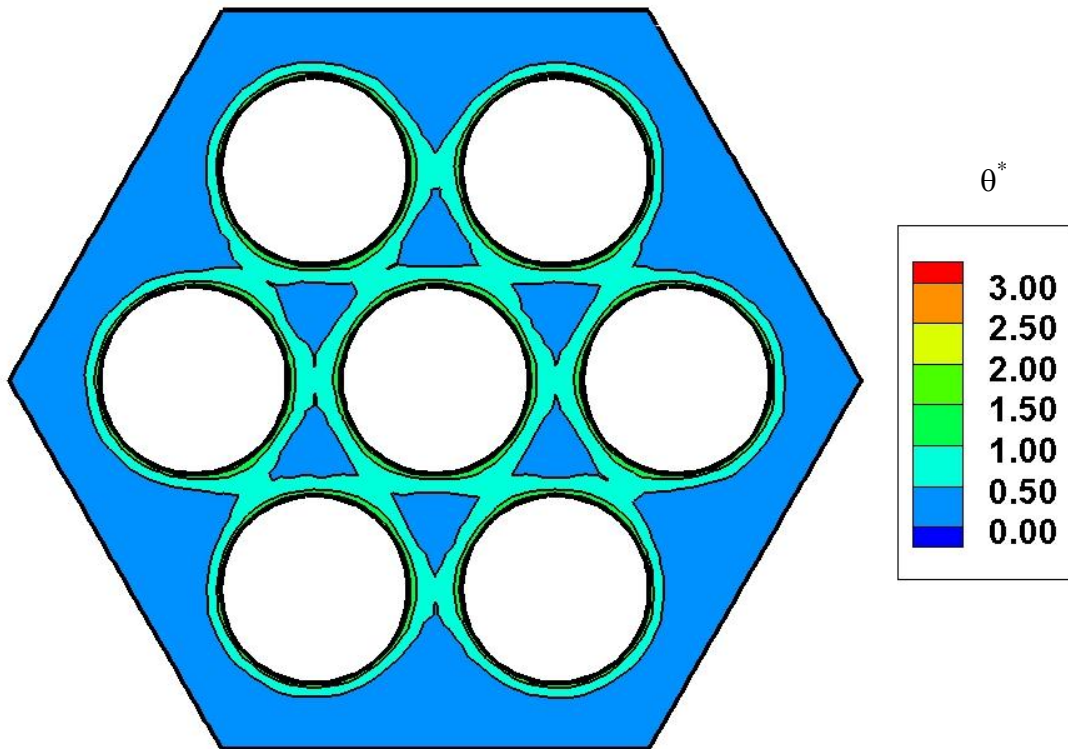


Fig.17 θ^* contour for bare tube bundle at axial location of $x/p=1$ for the configuration of $P/d=30.30$, $P_v/d=1.34, D/d=4.5$

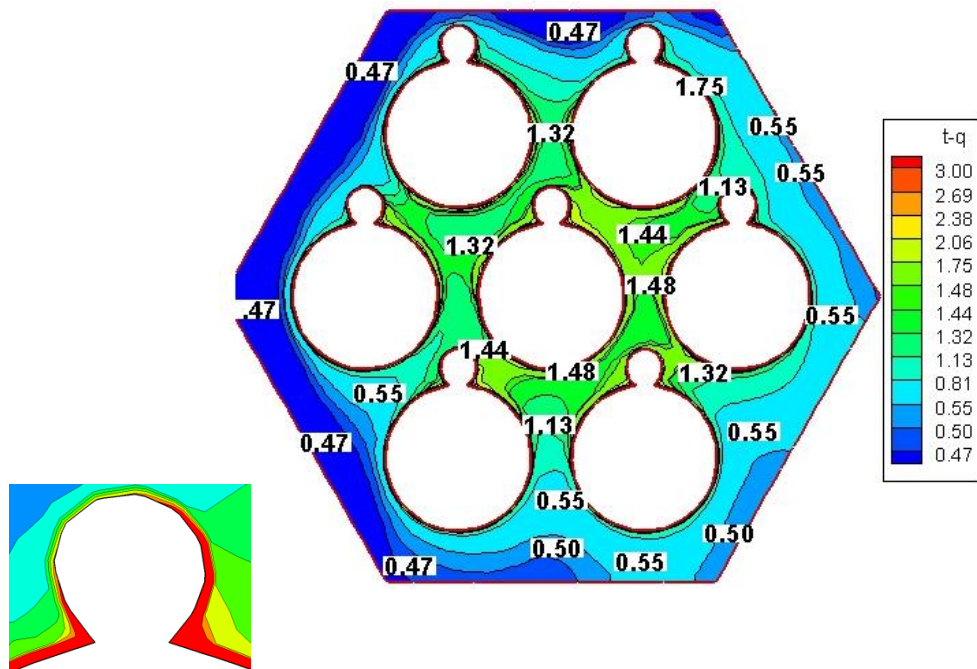


Fig.18 θ^* contour for bare tube bundle at axial location of $x/p=1$ for the configuration of $P/d=30.30$, $P_v/d=1.34, D/d=4.5$

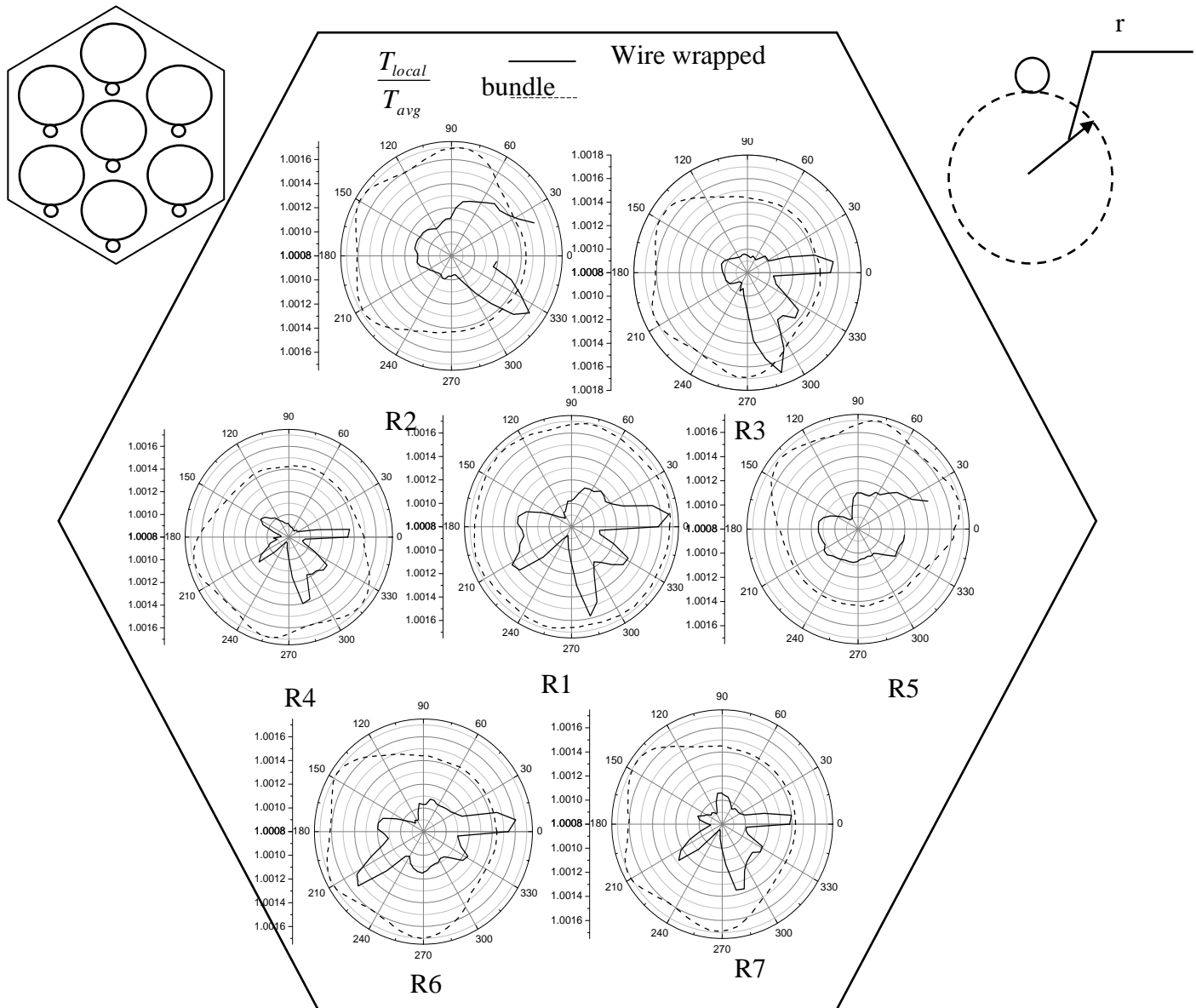


Fig.19 Comparison of T_{local}/T_{avg} distributions for wire-wrapped & bare tube bundle at axial location of $x/p=0.5$ and radial location of mid of the helically wrapped wire diameter for the configuration of $P/d=30.30$, $P_w/d=1.34$, $D/d=4.5$

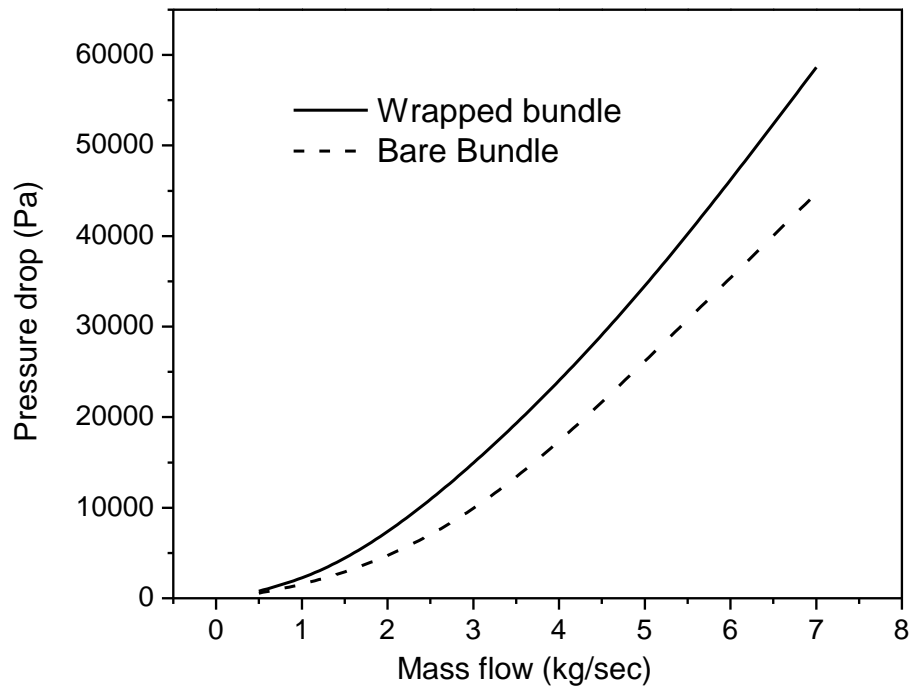


Fig.20 Effect of wire on pressure drop for bare and wrapped wire tube bundle

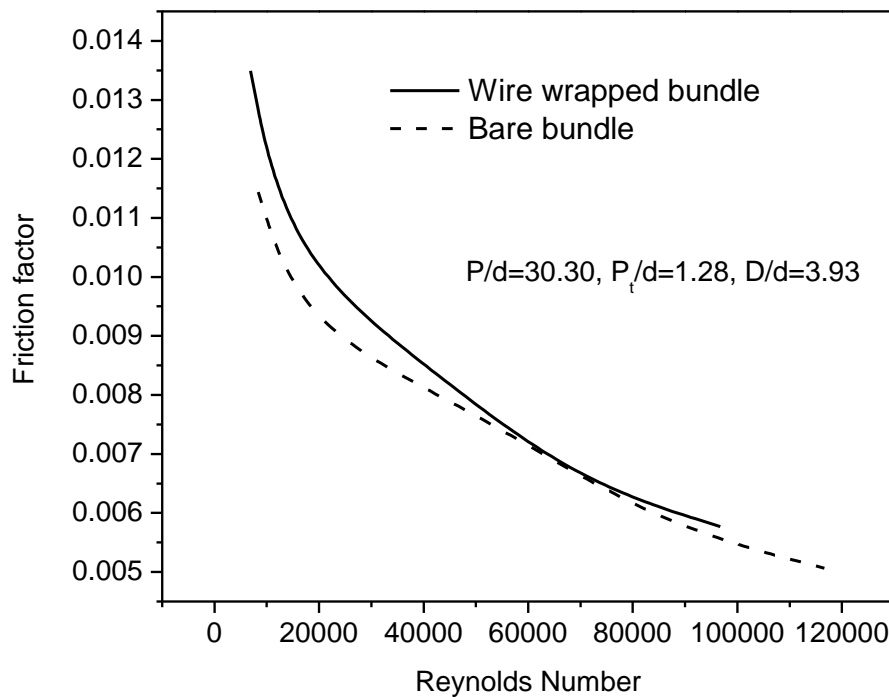


Fig.21 Effect of wire on friction factor for bare and wrapped wire tube bundle

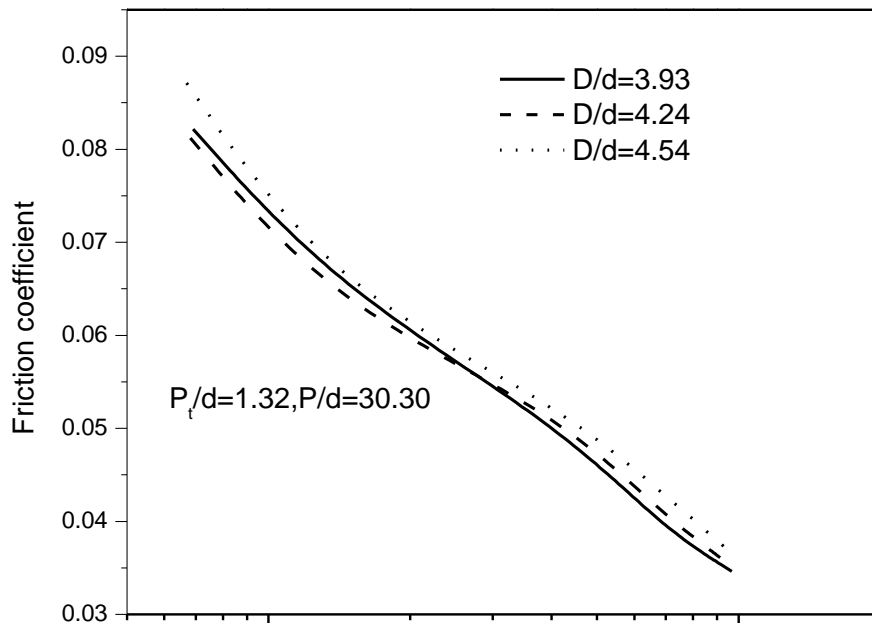


Fig.22 Effect of diameter ratio on friction factor in helically wrapped wire tube bundle

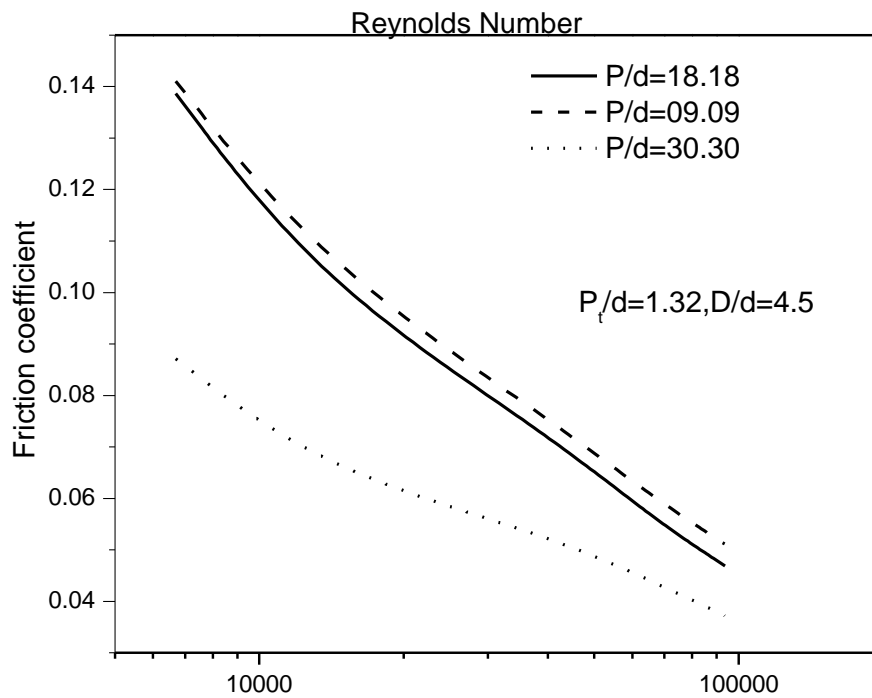


Fig.23 Effect of Helical pitch ratio on friction factor in helically wrapped wire tube bundle

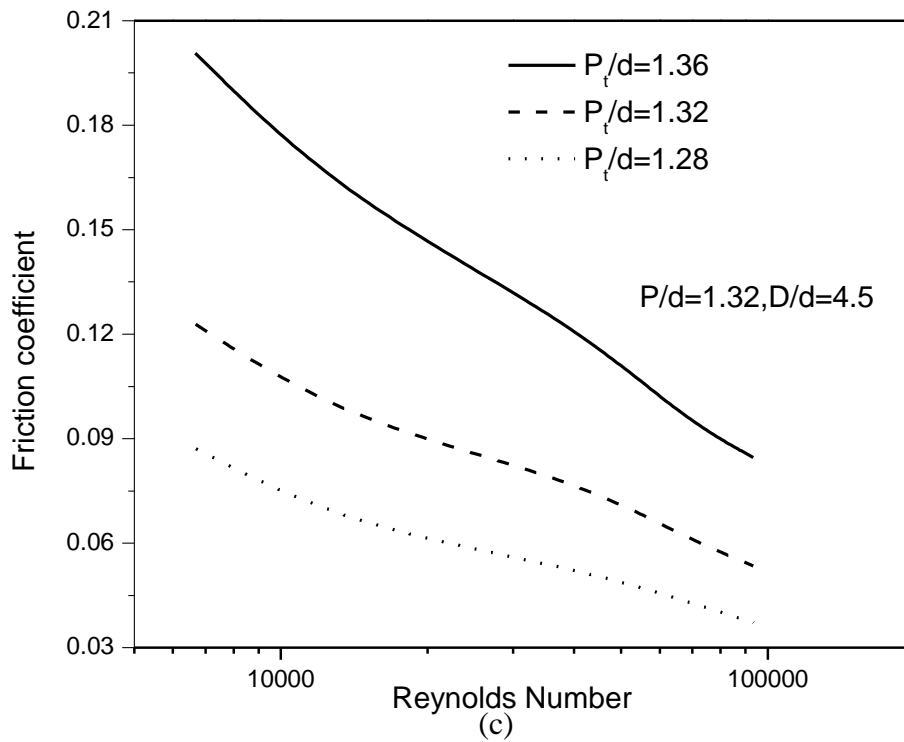


Fig.24 Effect of triangle pitch ratio on friction factor in helically wrapped wire tube bundle

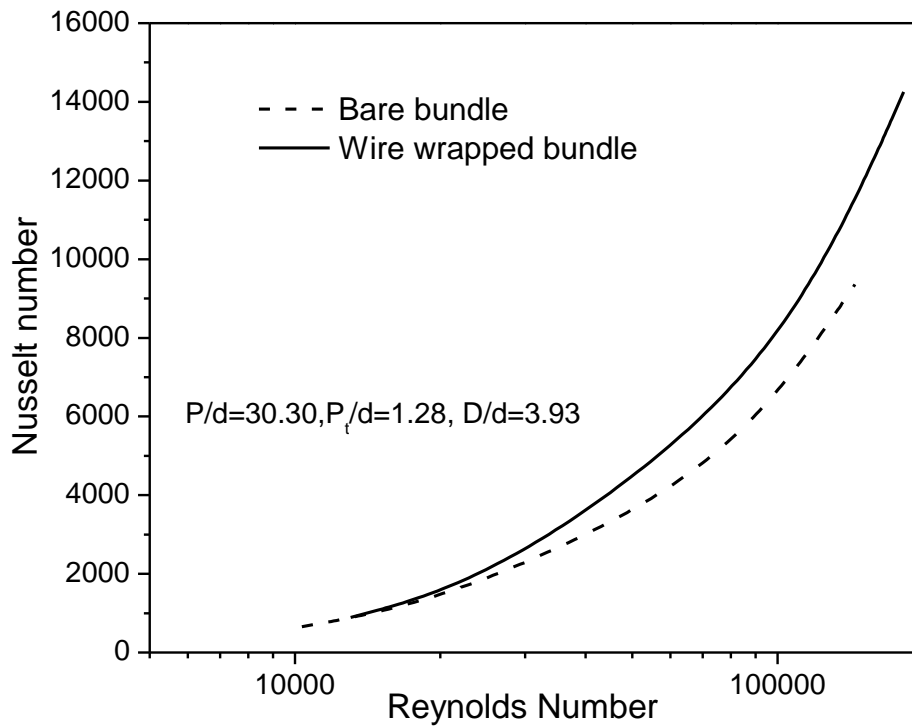


Fig.25 Effect of helically wrapped wire insert on Nusselt number in bare tube bundle

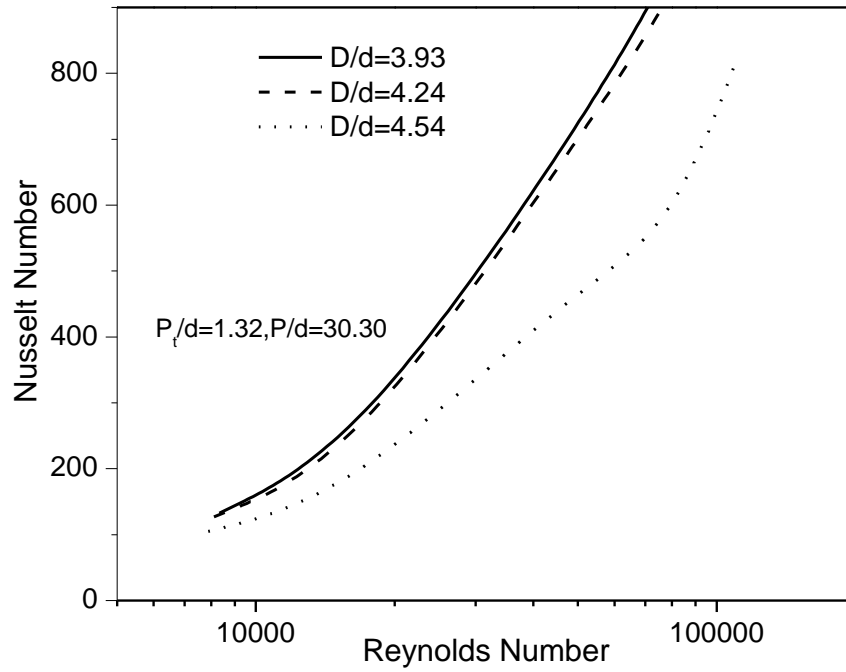


Fig.26 Effect of diameter ratio on Nusselt number in helically wrapped wire tube bundle

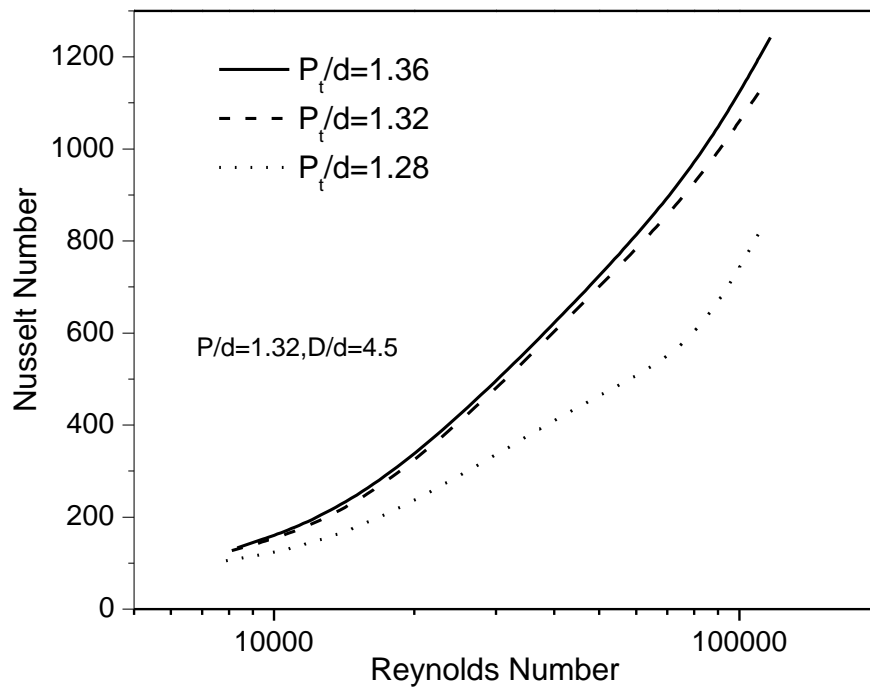


Fig.27 Effect of helical pitch ratio on Nusselt number in helically wrapped wire tube bundle

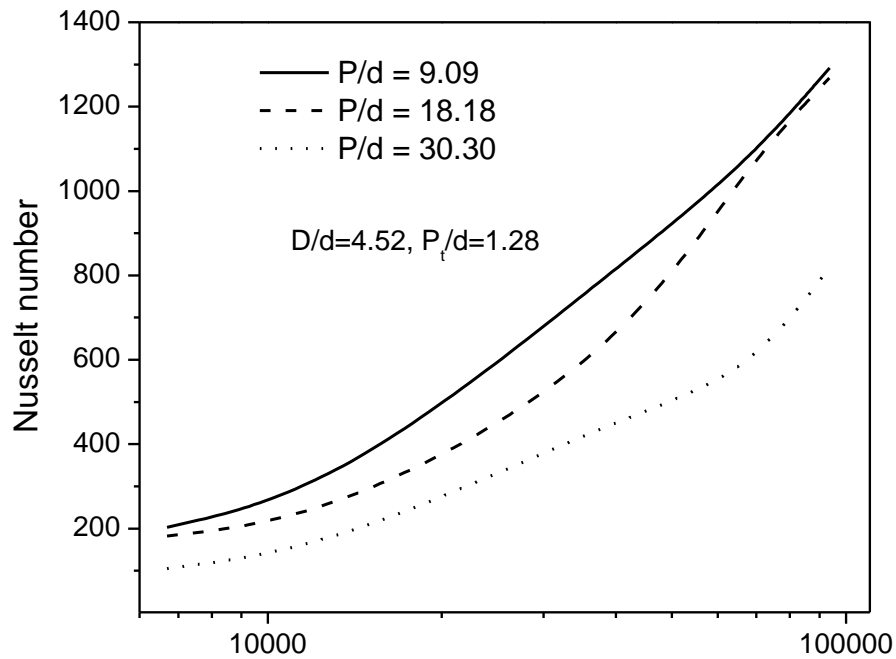


Fig.28 Effect of triangular pitch ratio on Nusselt number in helically wrapped wire tube bundle

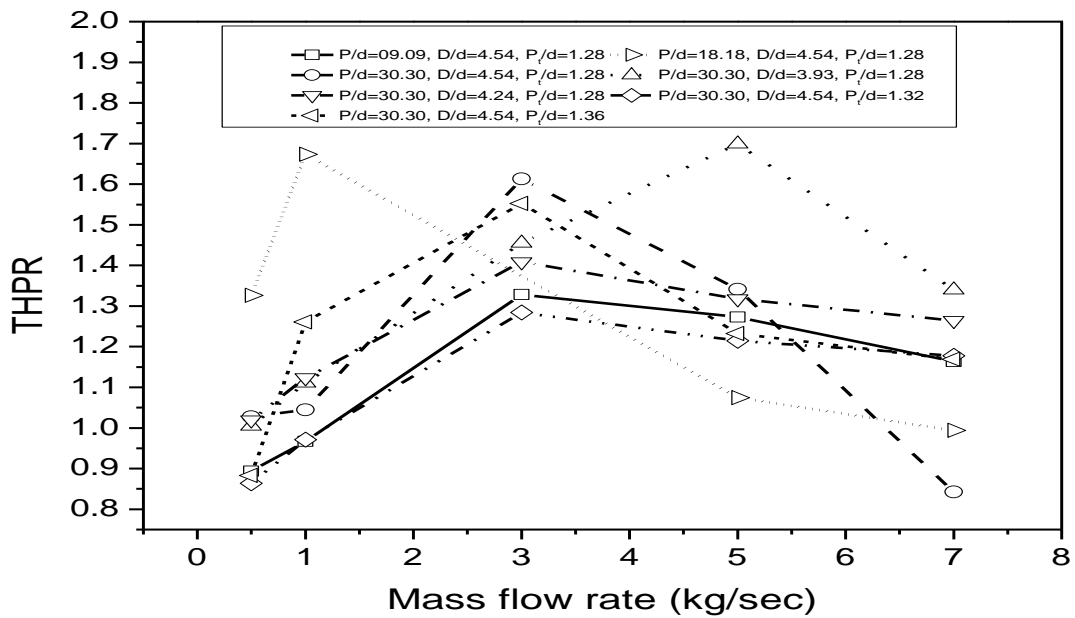


Fig.29 Comparison of THPR for all configurations to choose best configuration in the wrapped wire tube bundle

Table 1 Friction factor correlations for wire-wrapped bundle

S.No	Authors	Type	Correlation
1	Eifler and Nijssing [6]	Triangular array of parallel rods	$f = \frac{A_m^3}{P_e'} \left[\Delta P_i \frac{2}{\rho Q_v^2} + \frac{1}{A_2^2} - \frac{1}{A_1^2} \right]$
2	Grillo and Marinelli [7]	4 x 4 array rod bundle	$f = 0.1626 \text{Re}^{-0.2}$
3	Novendstern [8]	217 pin bundle with wire wrap system	$\Delta P = f \frac{L}{D_e} \frac{\rho V^2}{2} \text{ where } f = f_1 X_1^2 \frac{D_e}{D_{e1}}; f_1 = f_s M; f_s = \frac{0.316}{\text{Re}_1^{0.25}}$ $M = \left\{ \frac{1.034}{\left(\frac{P}{D}\right)^{0.124}} + 29.7 \frac{\left(\frac{P}{D}\right)^{6.94} \text{Re}_1^{0.086}}{\left(\frac{H}{D}\right)^{2.239}} \right\}^{0.885}; \text{Re}_1 = \frac{\rho V_1 D_{e1}}{\mu} = \text{Re} X_1 \frac{D_{e1}}{D_e}$ $\text{Re} = \frac{\rho V D_e}{\mu}; V_1 = X V$ $X_1 = \frac{A}{N_1 A_1 + N_2 A_2 \left(\frac{D_{e2}}{D_{e1}}\right)^{0.714} + N_3 A_3 \left(\frac{D_{e3}}{D_{e1}}\right)^{0.714}}$ $A = N_1 A_1 + N_2 A_2 + N_3 A_3$
4	Rehme [9]	7X37 wire wrap bundle	$f = \left(\frac{64}{\text{Re}} F^{0.5} + \frac{0.0816}{\text{Re}^{0.133}} F^{0.9335} \right) N_r \pi \left(\frac{D + D_w}{S_t} \right)^{2.16}$ <p>where</p> $F = \left(\frac{P}{D} \right)^{0.5} + \left[7.6 \left(\frac{D + D_w}{H} \right) \left(\frac{P}{D} \right)^2 \right]^{2.16}$

5	Engel, Markley and Bishop [10]		$f = \frac{110}{Re} \text{ for } Re \leq 400$ $f = \frac{110}{Re} (1-\psi)^{0.5} + \frac{0.55}{Re^{0.23}} \psi^{0.5} \quad 400 \leq Re \leq 5000$ $f = \frac{0.55}{Re^{0.25}} \text{ for } 5000 \leq Re$ <p>where</p> $\psi = \left(\frac{Re-400}{4600} \right)$
6	Arwlkar and Fenech [11]	61 rod bundle	$f = 25.72 (Nre)^{-0.835} \text{ for } Nre < 1000,$ $f = 0.436 (Nre)^{-0.263} \text{ for } 2000 < Nre < 25000$
6	Cheng and Todreas [5]	37 pin rod bundle with wire wrap	$f = \frac{C_{fT}}{Re^{0.18}} \quad Re \geq Re_T \quad \quad \quad f = \frac{C_{fL}}{Re} \quad Re \leq Re_L$ $f = \frac{C_{fL}}{Re} (1-\psi)^{\frac{1}{3}} + \frac{C_{fT}}{Re^{0.18}} \psi^{\frac{1}{3}} \quad Re_L \leq Re \leq Re_T$ $\log\left(\frac{Re_L}{300}\right) = 1.7\left(\frac{P}{D} - 1.0\right)$ $\log\left(\frac{Re_T}{10000}\right) = 0.7\left(\frac{P}{D} - 1.0\right)$ $\psi = \frac{\left(\log(Re) - \left(1.7\frac{P}{D} + 0.78\right)\right)}{\left(2.52 - \frac{P}{D}\right)}$ $C_{fL} = \left(-974.6 + 1612.0\left(\frac{P}{D}\right) - 598.5\left(\frac{P}{D}\right)^2 \left(\frac{H}{D}\right)^{0.06-0.085\left(\frac{P}{D}\right)} \right)$ $C_{fT} = \left(0.8063 - 0.9022\log\left(\frac{H}{D}\right) + 0.3526\left(\log\left(\frac{H}{D}\right)^2\right)\left(\frac{H}{D}\right)^{1.78-2\left(\frac{P}{D}\right)}\left(\frac{P}{D}\right)^{9.7} \right)$

7	Carajilescov and Fernandez [12]	Bundles with up to 61 rods with wire wrap	$V_1 = \psi V_1^*$ $\psi = \frac{1}{\cos \alpha}$ where α is angle between rod axis and flow direction $A_i^* = \frac{A_i}{\psi}$ the length followed by fluid, in wire lead is: $H^* = \psi H \quad H = \text{wire lead} \quad A_w = P_{wl} H = P_{wl}^* H^*$ $\Delta P = f_1 \frac{H}{D_{el}} \frac{\rho V_1^2}{2} = f_1^* \frac{H^*}{D_{el}^*} \frac{\rho V_1^{*2}}{2} \quad \overline{f_1} = M_1 \text{Re}_1^{s_1}$ $D_{el}^* = \frac{4A_i^*}{P_{wl}^*} \quad M_1 = M_1^* \psi^{3+s_1}$
8	Vijayan, Pilkhwal, Saha and Venkat Raj [13]	52 wire wrap rod bundle	$f = 0.5529 \text{Re}^{-0.30205}$
9	Seok Ki Choi, Kon Choi, Ho Yun Nam and Hoon Ki Choi [14]	271 pin fuel sub assembly of liquid metal reactor	The measured pressure drop data using four correlations. It is shown that the correlation proposed by Cheng and Todreas fits best with the present experimental data among the four correlations considered.

10	Holloway, McClusky, Beasley and Conner [15]	5X5 rod bundle with support grid features	$f = \Delta P_{rod} \frac{D_e}{\Delta Z_{rod}} \left(\frac{\rho V^2}{2} \right)$ $\Delta P_g = \Delta P_{grid} - \frac{\Delta Z_{grid}}{\Delta Z_{rod}} \Delta P_{rod}$ $\Delta P_g = \text{Pressure drop due sole to the grid}$
11	Sobolev, V. [16]		$f = (1 + 600 \left(\frac{D_r}{H} \right)^2 \left(\frac{P_t}{D_r} - 1 \right) \times \left(\frac{0.210}{\text{Re}^{0.25}} \left(\frac{P_t}{D_r} - 1 \right)^{0.32} \right)$
11	Vijayan, Pilkhwal, Saha, and Venkat Raj [17]	51 rod bundle	$f = 0.236 f^{-0.17}$

Table.2 Mesh size and maximum wall Y plus of Inner wall for different configurations

Configuration			Mesh Size	Maximum wall y^+ for wire-wrapped bundle
D/d	P/d	Pt/d		
4.44	30.3	1.28	31,50,887	4.95
4.24	30.3	1.28	28,20,078	4.8
3.93	30.3	1.28	26,30,496	4.3
4.44	18.18	1.28	18,897,68	4.2
4.44	9.09	1.28	13,222,68	1.86
4.44	30.3	1.32	32,62,484	4.8
4.44	30.3	1.36	32,88,996	4.92